Seismic Behavior and Design of Unbonded Post-Tensioned Precast Concrete Frames

Magdy T. El-Sheikh, Ph.D.
Lecturer
Department of Structural Engineering
Cairo University
Cairo, Egypt

Richard Sause, Ph.D., P.E.
Associate Professor
Department of Civil and Environmental Engineering
Lehigh University
Bethlehem, Pennsylvania

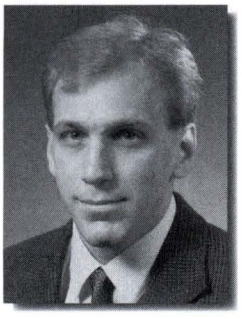

Stephen Pessiki, Ph.D.
Associate Professor
Department of Civil and Environmental Engineering
Lehigh University
Bethlehem, Pennsylvania

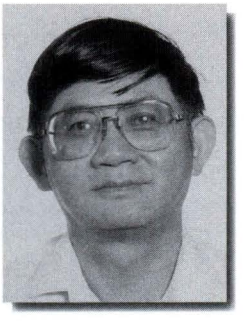

Le-Wu Lu, Ph.D.
Professor
Department of Civil and Environmental Engineering
Lehigh University
Bethlehem, Pennsylvania

Unbonded post-tensioned precast concrete beam-column subassemblages have been studied in previous research and were found to be a promising seismic resistant structural system. The behavior of two six-story unbonded post-tensioned frames is studied using nonlinear push-over static analyses and time-history dynamic analyses. Two analytical models are developed for the analyses; the fiber model and the spring model. The results show that the behavior of unbonded post-tensioned precast frames, in particular, the strength, ductility, and self-centering capability, is more than adequate for severe earthquake loading.

Precast concrete structural systems for buildings are cost-efficient systems which provide high quality, and fast, easy erection on site. However, the research performed on precast concrete structural systems is limited compared to research on reinforced concrete systems. As a result, the U.S. model building codes include detailed seismic design provisions for cast-in-place reinforced concrete structural systems, but include only general provisions for the design of precast concrete structural systems.

In response to the recognized need for research on precast concrete systems for seismic regions, the PRESSS (Precast Seismic Structural Systems) research program was initiated in 1990.[1] The PRESSS research program is a coordinated program of analytical and experimental research intended to develop seismic resistant structural systems and seismic design provisions for precast concrete structures. The research described in this paper was performed as part of the PRESSS program.

This paper focuses on unbonded post-tensioned precast concrete frames. Prototype frames are discussed first. Then, the behavior of beam-column connections/subassemblages is discussed. Criteria are then proposed for the design of unbonded post-tensioned precast frames. The design of the prototype frames according to the design criteria is then discussed. Finally, the results of static and dynamic analyses of the prototype frames are presented and discussed.

SELECTION OF PROTOTYPE FRAMES

The prototype structures investigated in this paper are six-story office buildings. The layout of the lateral and gravity load frames of the prototype structures is shown in Fig. 1(a). An elevation view showing the story heights and precast concrete components is given in Fig. 1(b). The building layout is adopted from the layout suggested by Nakaki and Englekirk.[2]

The lateral load system is comprised of four unbonded post-tensioned precast frames, two for each direction, located on the perimeter of the plan. The lateral load resisting frames (prototype frames) also carry gravity loads. The floor system consists of 24 in. (610 mm) deep double tees running in the north-south direction of the building. The floor system is provided with a 2.5 in. (64 mm) thick cast-in-place concrete topping.

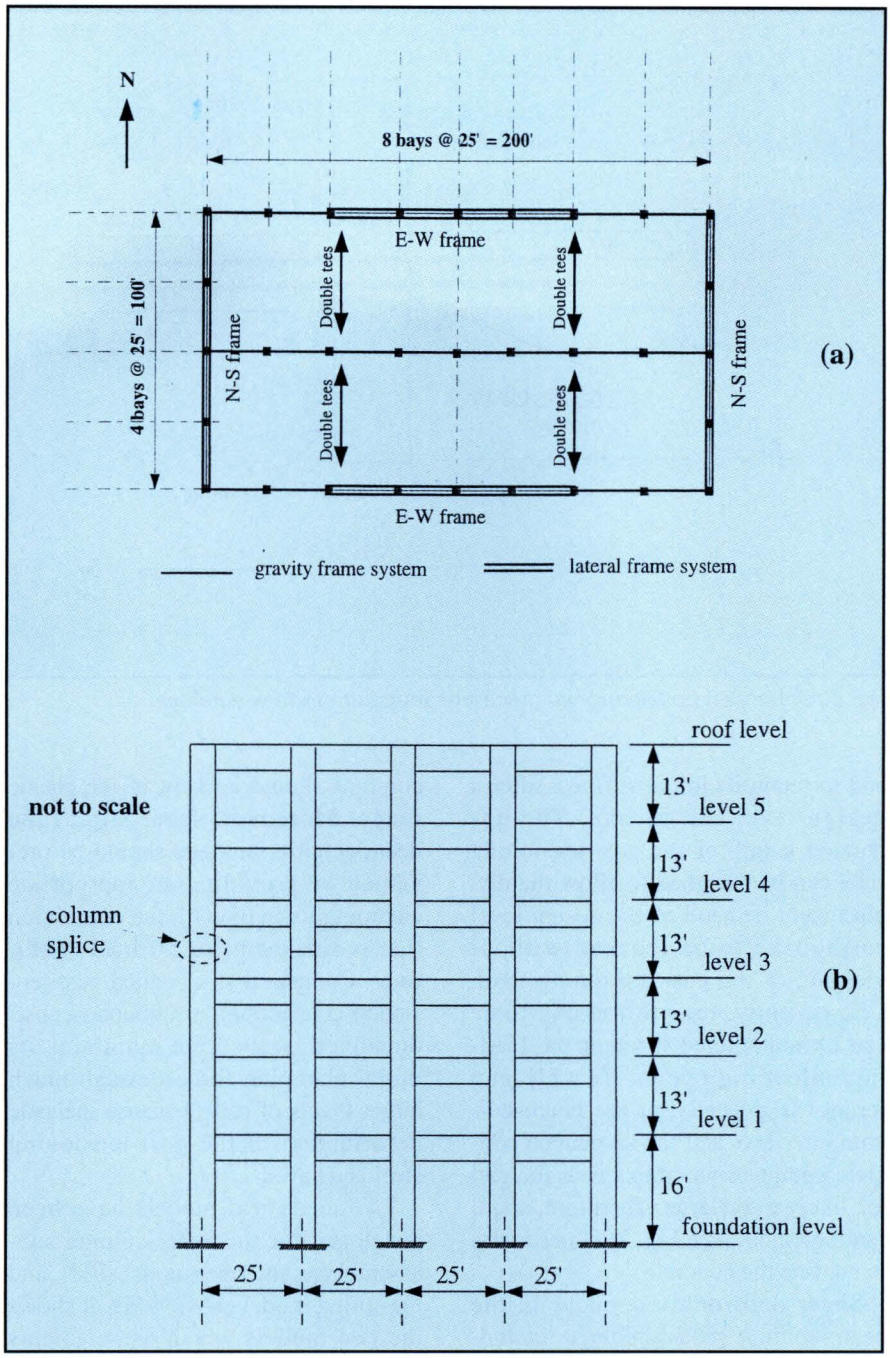

Fig. 1. Prototype frames: (a) layout of prototype building; (b) elevation view of prototype frames. **Note:** 1 ft = 305 mm.

SUBASSEMBLAGE BEHAVIOR AND MODELING

Unbonded post-tensioned precast concrete frames are designed as "ductile frames," in which the nonlinear/inelastic deformations occur only in the connections. Therefore, the frame behavior is controlled by the beam-column connection behavior. To investigate the beam-column connection behavior, a subassemblage is cut from the frame at the locations of hypothetical points of inflection located at midheight of the columns and midspan of the beams (see Fig. 2).

The subassemblage consists of connected beam and column segments with boundary conditions typical of beam-column subassemblage test specimens. The beam-column connection is considered to be the part of the beam adjacent to the column. The post-tensioning steel is unbonded through the column and for some distance through the beams on each side.

The flexural behavior of an unbonded post-tensioned beam-column connection is characterized by gap opening/closing at the beam-column interface upon loading/unloading. Unlike cast-in-place connections, the inelastic deformations are concentrated in the connection region where a "crack" already exists between the precast beam and column segments. In addition, because the post-tensioning steel is unbonded, additional flexural cracks do not form in the beam in the connection region.

The load-deflection behavior of the subassemblage is essentially nonlinear elastic as shown in Fig. 3. Although this behavior provides little energy dissipation, a frame utilizing this type of connection can be designed to return to its original position without residual displacement (self-centering)

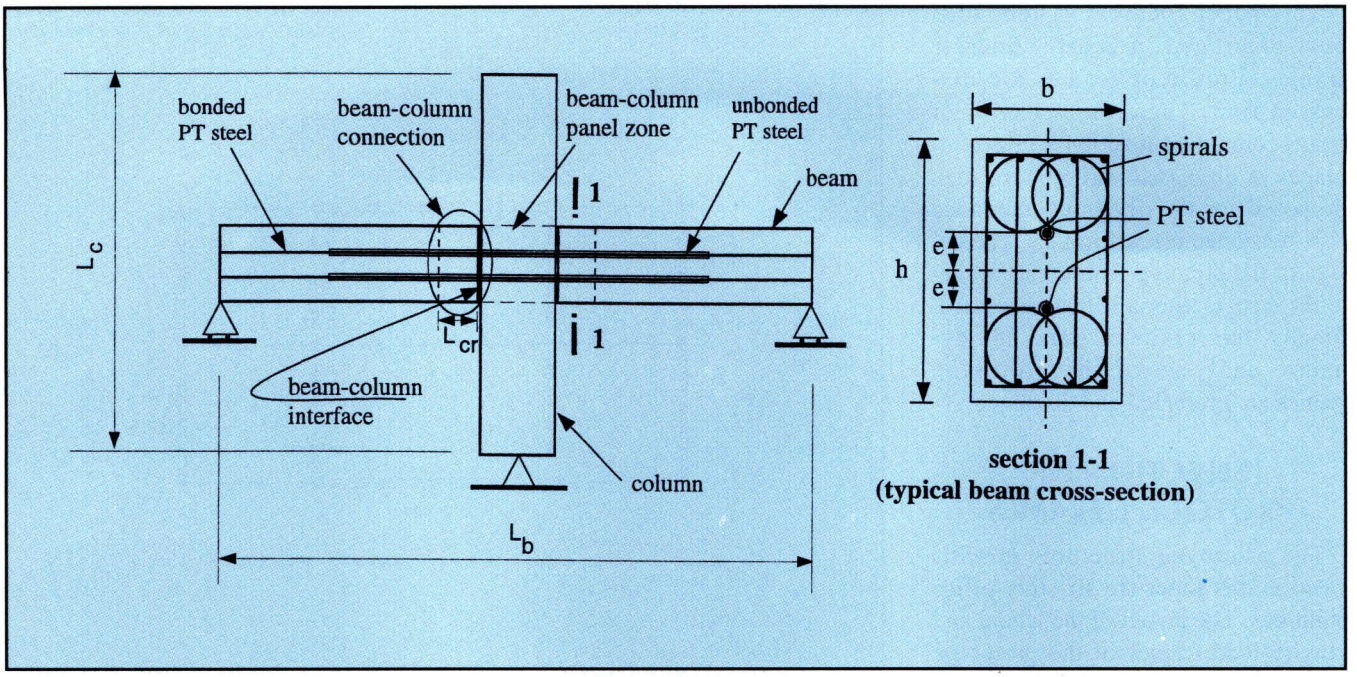

Fig. 2. Unbonded post-tensioned precast beam-column subassemblage.

and to retain its initial stiffness after a design level earthquake. The unbonded length of the post-tensioning steel can be designed to allow the displacement demand of the design level earthquake to be reached without yielding of the post-tensioning steel. Consequently, the prestressing force can be maintained through the loading/unloading cycles. A wide gap (crack) is expected at the beam-column interface, and the associated concrete compression strains near the gap are likely to be large. Therefore, spiral reinforcement (see Fig. 2) is necessary to confine the concrete.

Shear deformations occur in the beam-column subassemblage, including the beam-column panel zone. Shear deformations in the beams and columns should be kept in the elastic range. Moreover, shear slip at the beam-column interface should be prevented by providing an appropriate clamping force through the connection that is sufficient for all load conditions. Compared to a bonded post-tensioned connection, an unbonded post-tensioned connection maintains its initial clamping force through much larger levels of drift, because inelastic deformation of the post-tensioning steel is delayed.

Two analytical models have been developed for the beam-column subassemblage: the fiber model (FM), and the spring model (SM).[3,4] Fig. 4 shows the two models which use elements from the computer program DRAIN-2DX.[5]

Fig. 3. Nonlinear elastic load-deflection behavior.

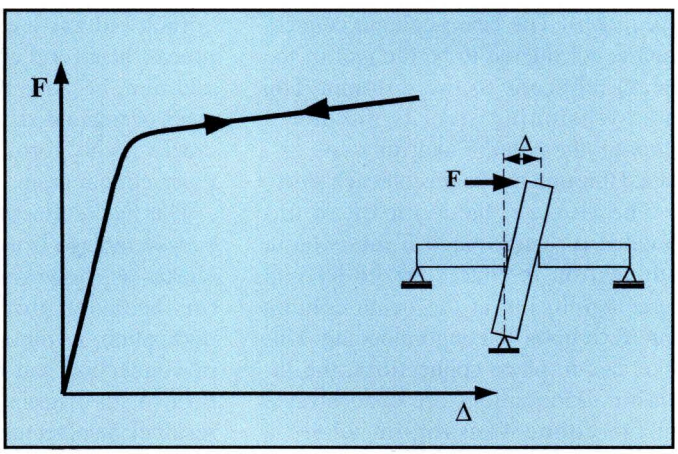

In the FM, the behavior of the concrete in the beam-column connection region is modeled using fiber beam-column elements. Other elements used in the FM include: (1) elastic beam-column elements to model parts of the beams and columns where only linear elastic deformations are expected to occur; (2) truss elements to model the unbonded post-tensioning steel; (3) a zero-length spring element to model the panel zone shear deformations; (4) rigid links and rigid end zones to model the axial and flexural deformations of the portions of the beams and columns within the panel zone, respectively; and (5) rigid links to tie the truss element end nodes to the adjacent fiber nodes at the locations of the post-tensioning steel anchorages.

In the SM, the nonlinear behavior of an unbonded post-tensioned precast beam-column connection is modeled using a zero-length rotational spring element, which replaces the fiber and truss elements in the FM. The SM is expected to give less accurate results than the FM. However, the hysteretic behavior of the SM can be directly controlled varying a factor (α_r), unlike the hysteretic behavior of the FM, which depends directly on the behavior of the concrete and steel fibers used to model the beam cross section. This feature of the SM is used in parametric studies of the dynamic response

of the prototype frames, as discussed later.

The FM and the SM are verified by comparing their behavior with the results of a test conducted at NIST on Specimen GPZ4.[6] Fig. 5(a) shows the experimentally determined hysteretic behavior of NIST Specimen GPZ4, plotted as lateral load versus lateral deflection. Figs. 5(b) and (c) show the hysteretic behavior of this specimen predicted by analysis using the FM and the SM, respectively.

Both models provide a good estimate of the hysteretic behavior of the test specimen. In particular, the initial stiffness and the strength are accurately predicted by both models. The hysteresis loops of the analytical models appeared to be narrower than the test results which indicates that the models underestimate the energy dissipation of the specimen.

BEHAVIOR OF BEAM-COLUMN CONNECTIONS

The moment-rotation behavior of an unbonded post-tensioned beam-column connection is characterized by several limit states, which are related to the stress-strain state of the concrete and the stress-strain state of the post-tensioning steel. The following discussion is based on studies of a large number of unbonded post-tensioned beam-column connections.[3,4]

Fig. 6 shows the typical moment-rotation behavior of a connection designed to have yielding of the post-tensioning steel before failure (crushing) of the confined concrete. Fig. 6 also shows a trilinear idealization of the moment-rotation behavior. Five limit states are identified.

State 1 is the decompression limit state. It represents the beginning of gap opening at the beam-column interface, when the concrete reaches zero stress at the extreme fiber of the beam. Increasing the moment beyond the decompression moment (M_{dec}) causes: (1) an initiation of gap opening and an increase in the length of the gap opening along the interface which results in geometric softening of the connection; and (2) an increase in the stress and strain in the concrete which eventually

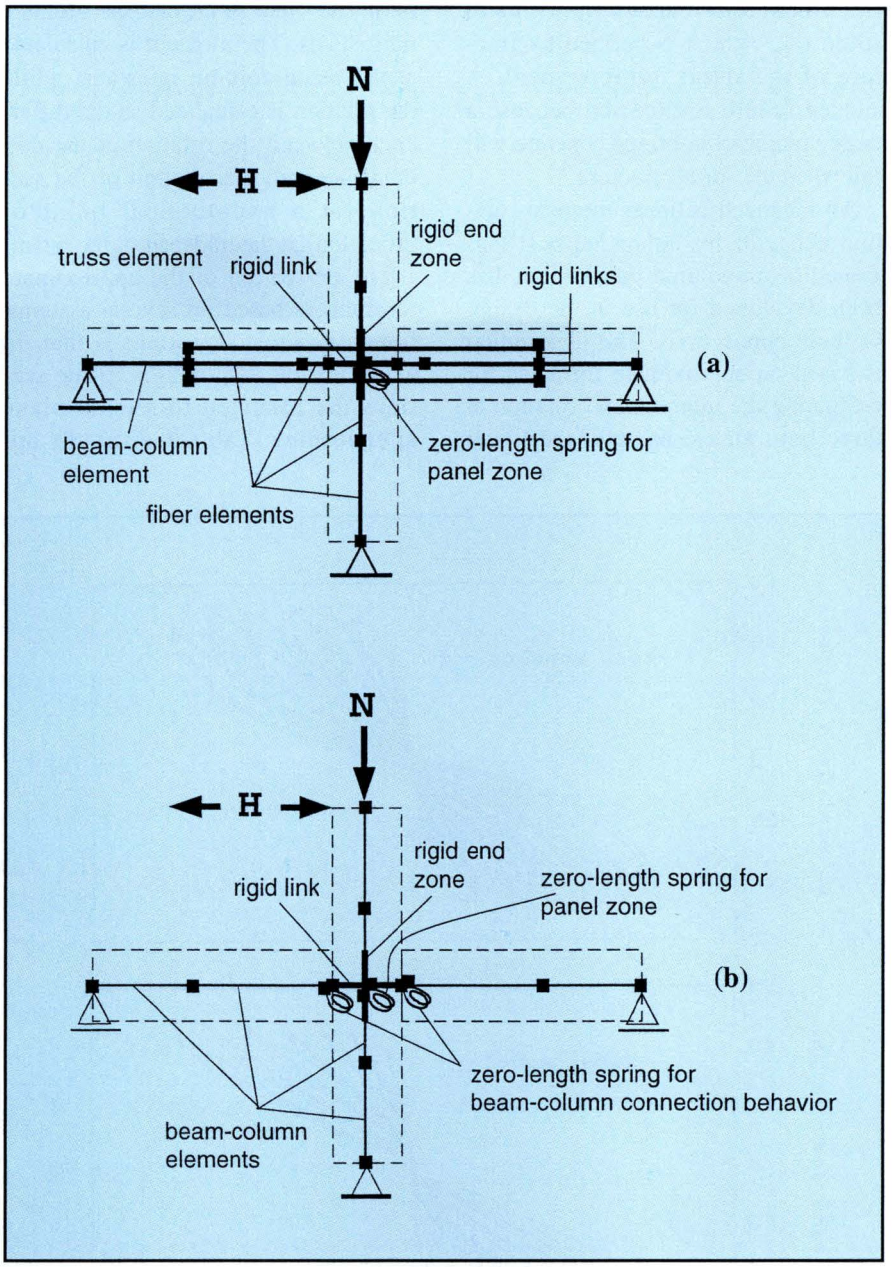

Fig. 4. Analytical models: (a) fiber model (FM); (b) spring model (SM).

results in concrete softening. Both of these effects gradually soften the moment-rotation behavior of the beam-column connection.

State 2 is the linear limit state (M_{ll},θ_{ll}). This is the state at which the moment-rotation behavior significantly deviates from the initially linear behavior and begins to soften dramatically. The linear limit is not well defined in terms of the stress-strain state of the concrete or the post-tensioning steel.

State 3 is the cover spalling limit state. This is the state at which the unconfined concrete cover spalls. At this state, a rapid decrease in the unconfined concrete stress takes place, causing a decrease in the slope of the beam moment-rotation relationship.

State 4 is the yield limit state (M_y,θ_y). This is the state at which the post-tensioning steel reaches the limit of proportionality (f_{pl}) on the post-tensioning steel stress-strain curve. The yield limit state is the upper bound on the elastic behavior of the beam-column connection. Beyond this state, the post-tensioning steel deforms inelastically, but the inelastic strain in the post-tensioning steel is small, because the inelastic strain is spread over the unbonded length.

State 5 is the ultimate limit state (M_{ult},θ_{ult}). This is the state when the strain in the extreme fiber of the con-

fined concrete reaches its ultimate strain (ε_{cu}) which is defined by fracture of the spiral reinforcement. A sudden failure is expected because a large volume of confined concrete will fail when the spirals fracture.

An idealized trilinear moment-rotation behavior for unbonded post-tensioned beam-column connections has been developed for use in the design of these connections. The idealization is based on approximate formulas for estimating the moment and rotation at three limit states, namely, the linear limit, the yield limit, and the ultimate limit states. The moment is calculated at the beam-column interface, while the rotation is calculated as the difference between the rotation at the column face and the rotation of the section (at a hypothetical point of inflection) at the midspan of the beam.

The derivation of the approximate formulas is based on several assumptions, the most important is that, in axial-flexural deformation, plane sections are assumed to remain plane after loading. Table 1 gives the approximate formulas used for the trilinear idealization. The detailed derivation of the approximate formulas can be found in the reports by El-Sheikh et al.[3,4]

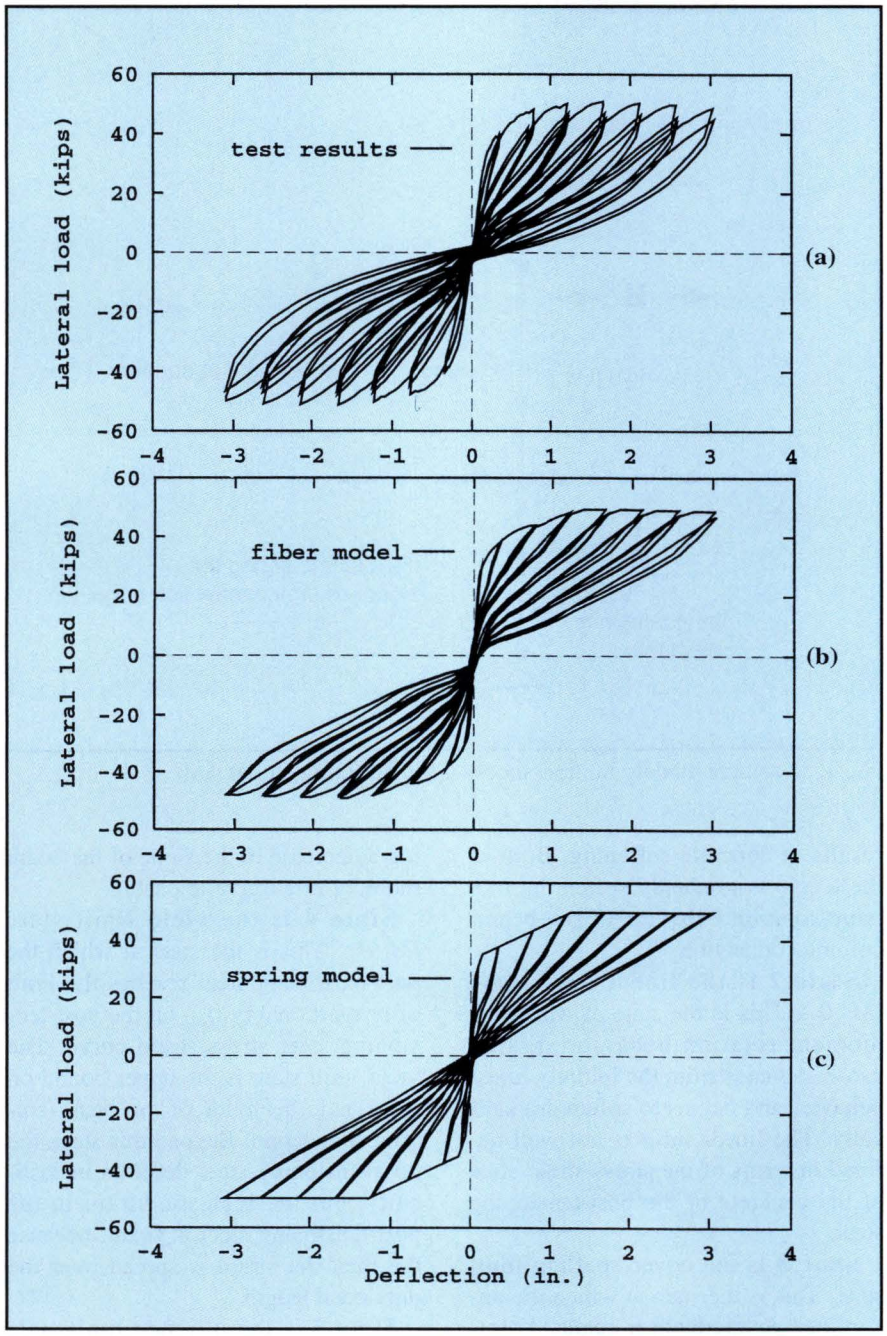

Fig. 5. Lateral load-deflection relationship for NIST Specimen GPZ4: (a) test results; (b) fiber model (FM); (c) spring model (SM). **Note:** 1 in. = 25.4 mm; 1 kip = 4.45 kN.

Estimation of the Linear Limit (M_{ll},θ_{ll}) — The linear limit moment (M_{ll}) is considered to be the smaller of two values; the first value accounts for concrete softening and the second value accounts for geometric softening due to gap opening. The first value of M_{ll} is the moment calculated by including the concrete cover, treating all the concrete as unconfined, assuming the extreme fiber strain of the concrete is 0.003, and assuming the force in the post-tensioning steel is the initial force (neglecting post-tensioning steel elongation). The second value of M_{ll} considers the opening of the gap at the beam-column interface. Typically, the effect of the gap opening on the slope of the moment-rotation curve is small until the gap opening length has propagated beyond the section centroid.[7]

Based upon studies of numerous beam-column connections using the fiber model, in which softening was not significant until the gap opening length propagated over 75 percent of the section depth, the linear limit moment which accounts for gap opening was selected to be $2.5M_{dec}$. The linear limit rotation (θ_{ll}) is calculated assuming the beam is uncracked, i.e., based on the initial stiffness of the moment-rotation curve.

Estimation of the Yield Limit (M_y,θ_y) — The estimation is based on several assumptions, the most important are: (1) the elastic flexural deformations over the length of the beam are negligible, since the rotation due to gap opening and deformation of the concrete near the beam-column interface is dominant, and the elastic deformations of the rest of the beam are small, (2) the center of rotation at the beam-column interface is at the neutral axis, and (3) the cover concrete has spalled.

Estimation of the Ultimate Limit (M_{ult},θ_{ult}) — Referring to Fig. 6, the beam ultimate moment (M_{ult}) is assumed equal to the yield moment (M_y). The main factors affecting the ultimate rotation capacity (θ_{ult}) are the ultimate concrete strain (ε_{cu}) and the

failure length of the confined concrete adjacent to the beam-column interface (L_{cr}) shown in Fig. 2. L_{cr} can be estimated from the dimensions of the confined concrete in compression in the beam-column connection at the ultimate limit. In this study, L_{cr} is taken as the minimum of the confined concrete width (b'') and two times the stress block depth ($2a''$). The curvature is assumed constant over L_{cr} and the elastic deformations over the remaining length of the beam are neglected.

PROPOSED DESIGN APPROACH

A proposed design approach, based on the equivalent lateral force procedure of the NEHRP seismic design provisions[8] is described in this section. To provide sufficient ductility, a frame is designed so the failure mechanism is a beam sway mechanism, where hinges form at the beam-column connections and at the bases of the columns. A capacity design concept is used to ensure that the remainder of the frame will remain linear elastic.

The proposed seismic design approach considers two levels of earthquake ground motion, the design level and the survival level. The design level ground motion is chosen to be the design basis ground motion of the 1991 and 1994 editions of the NEHRP provisions[8] with a 90 percent probability of not being exceeded in 50 years, corresponding approximately to a 500-year return period. The survival level ground motion is assumed to have a 90 percent probability of not being exceeded in 250 years, corresponding approximately to a 2500-year return period. The survival level ground motion is taken to be 2.5 times the NEHRP design basis ground motion.

According to the proposed design approach, the design level ground motion may cause only minor, easily repaired damage to both structural and nonstructural components, while the survival level ground motion may cause damage to the structure that cannot be repaired, but should not cause the structure to collapse.

The nonlinear behavior of a well-designed unbonded post-tensioned precast frame is controlled by the moment-rotation behavior of the beam-column connections. Therefore, the lateral load behavior of the frame is idealized using a trilinear base shear-roof displacement relationship based on the trilinear idealization of the moment-rotation behavior. The idealized base shear-roof displacement behavior is shown in Fig. 7, where three regions can be characterized. The first region is essentially linear elastic. The second region is characterized by a significantly reduced stiffness. The third region is a yielding plateau with essentially zero slope.

Three limit states are shown on the trilinear idealization of the frame behavior. The linear limit state (V_{ll},Δ_{ll}) corresponds to the effective linear limit of the frame which is controlled by the linear limit of the beam-column connections. The yield limit state (V_y,Δ_y) corresponds to an effective yield limit of the frame, when stresses in the post-tensioning steel in the beam-column connections reach the limit of proportionality of the steel.

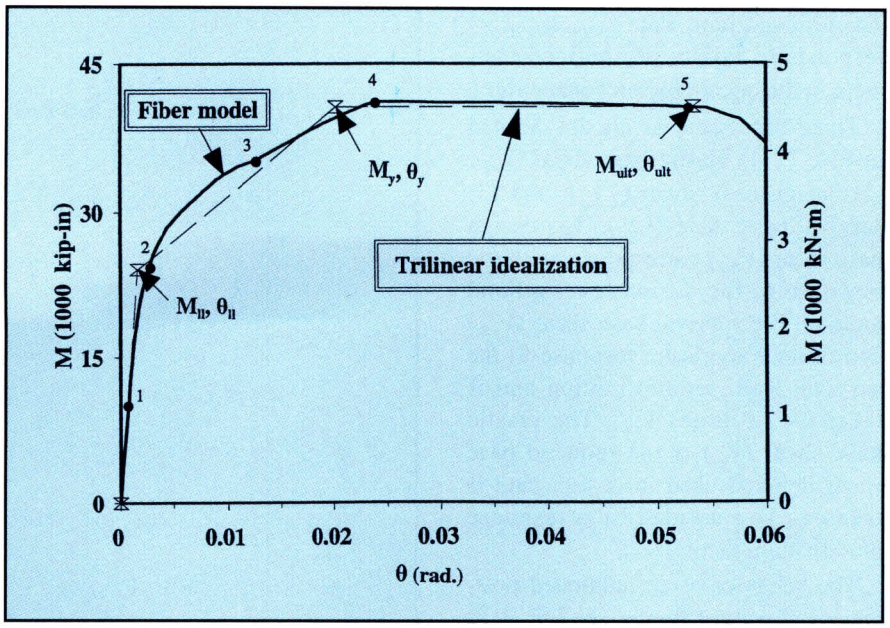

Fig. 6. Moment-rotation behavior of unbonded post-tensioned connection predicted by FM and proposed trilinear idealization. **Note:** 1 in. = 25.4 mm; 1 kip = 4.45 kN.

Table 1. Approximate formulas for moment-rotation behavior of beam-column connections.

Limit state	Moment	Rotation
Linear limit state	Smaller of the following: $M_{ll} = 0.50 f_{pi} A_p h \left(1 - \frac{f_{ci}/f_c'}{0.85}\right)$; $M_{ll} = 0.42 f_{pi} A_p h$	Smaller of the following: $\theta_{ll} = \frac{3L_{bc} f_{ci}}{2hE_c}\left(1 - \frac{f_{ci}/f_c'}{0.85}\right)$; $\theta_{ll} = \frac{2.5 L_{bc} f_{ci}}{2hE_c}$
Yield limit state *	$M_y = 0.5 f_{pl} A_p (h'' - a'')$; $a'' = \frac{c_1}{\alpha}\frac{f_{ci}/f_{cc}'}{f_{pi}/f_{pu}}\frac{b}{b''}h$	$\theta_y = \frac{(f_{pl} - f_{pi})L_{pu}}{(0.5h'' - a''/\beta)E_p}$
Ultimate limit state	$M_{ult} = M_y$	$\theta_{ult} = \frac{\varepsilon_{cu}\beta}{a''}L_{cr}$

Note: Notation is given in the Appendix.

* Approximate formulas for yield limit state are limited to interior beam-column connections and to exterior beam-column connections with concentric post-tensioning steel.

The ultimate limit state (V_{ult},Δ_{ult}) corresponds to failure of confined concrete in the beam-column connections.

Three base shear levels are defined in Fig. 7: (1) elastic base shear (V_{el}); (2) design base shear (V_{des}); and (3) survival base shear (V_{sur}). The design base shear (V_{des}) corresponds to elastic response to the design level ground motion. The survival base shear (V_{sur}) corresponds to elastic response to the survival level ground motion and is taken as 2.5 times V_{des}. The elastic base shear (V_{el}) is the reduced base shear demand used in design, and is taken as V_{des} divided by a response modification factor (R).

The behavior of an unbonded post-tensioned precast frame (see Fig. 7) is not easily predicted after the beam-column connections reach their linear limit, because the distribution of internal forces and deformations in the frame differs from the linear elastic distribution. This redistribution results in significant variations in the ductility demands among the beam-column connections, and the ductility demands on the beam-column connections are expected to be larger than the expected frame ductility demands.

The NEHRP[8] equivalent lateral force procedure idealizes seismic loading as static lateral forces. The force levels prescribed by the NEHRP design provisions are significantly lower than required to ensure a linear elastic response, as nonlinear behavior is allowed for economic reasons. The response modification factors (R) defined in NEHRP, are used to obtain reduced force levels (shown as V_{el} in Fig. 7) from the forces corresponding to linear elastic response to the design basis ground motion. The unbonded post-tensioned precast frame system is considered to be a special moment resisting frame system with ductile connections, and the corresponding value of $R = 8$ is used in design.

The proposed design approach uses the NEHRP equivalent lateral force procedure to determine the member forces and deformations. Design criteria for the flexural behavior of the beam-column connections are given below. Fig. 8 shows the idealized trilinear moment-rotation relationship for the beam-column connection, together with the notation used to describe the design criteria. The design approach has three sets of criteria related to the three limits of the trilinear idealization.

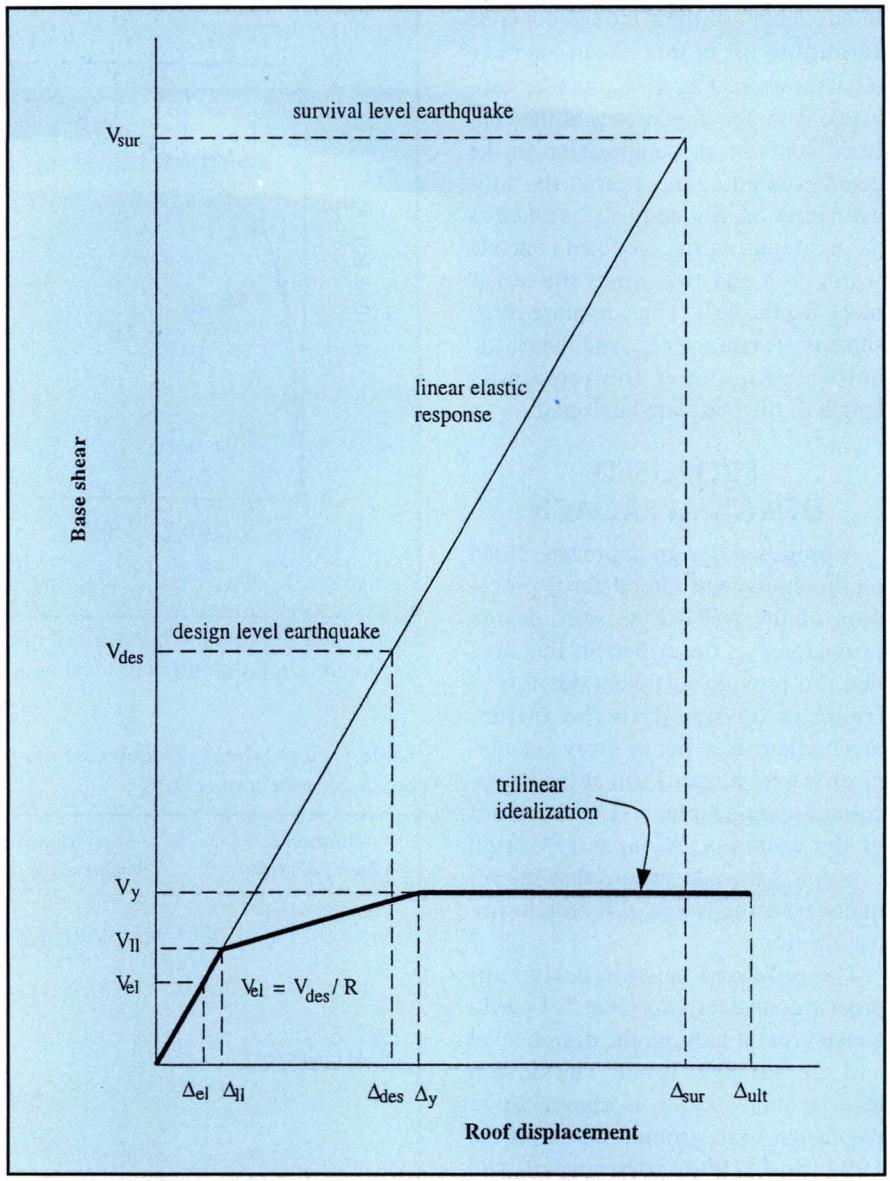

Fig. 7. Expected base shear-roof displacement behavior of unbonded post-tensioned precast frame.

Linear Limit State Criteria — The linear limit criteria are used to ensure that the connection has sufficient stiffness. The response of the beam-column connection up to the linear limit is essentially linear elastic. The linear limit criteria are defined in terms of both moment and rotation. The criterion for moment is:

$$M_{el} \leq M_{ll} \qquad (1)$$

where M_{el} is the beam-column connection bending moment demand for the reduced level of earthquake loading (shown as V_{el} in Fig. 7), estimated using linear elastic analysis of the frame under NEHRP[8] equivalent lateral forces (and factored gravity loads).

The linear limit criterion for rotation is related to the allowable story drift given in the NEHRP provisions.[8] Assuming that the story drift is mainly caused by the beam-column connection rotation, the criterion is written as follows:

$$\theta_{el} \leq \theta_{all} / C_d \qquad (2)$$

where

θ_{el} = beam-column connection rotation demand for the reduced level of earthquake loading, estimated using linear elastic analysis under NEHRP[8] equivalent lateral forces

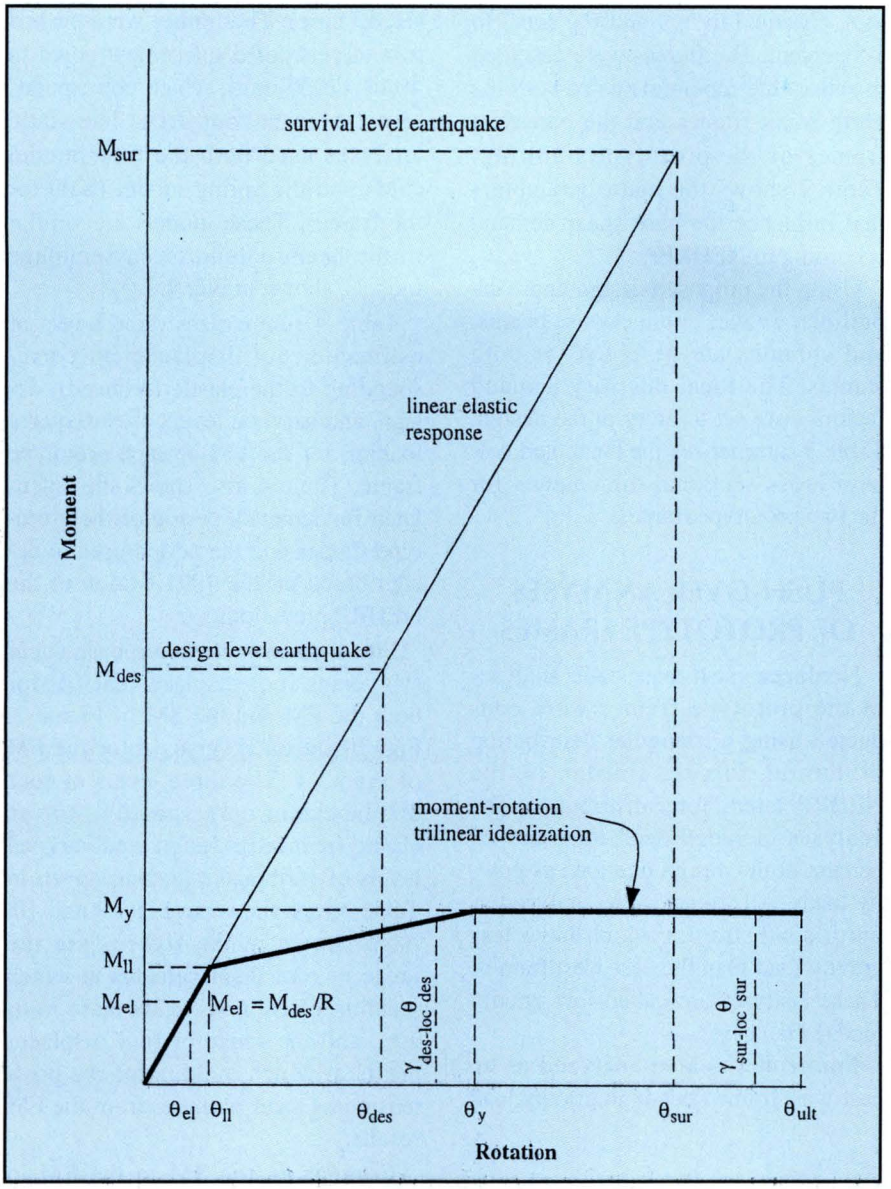

Fig. 8. Moment-rotation behavior of unbonded post-tensioned precast beam-column connection.

θ_{all} = allowable rotation which is taken as the allowable story drift of the NEHRP provisions[8]

C_d = NEHRP inelastic deflection amplification factor

The purpose of this criterion is to impose frame stiffness requirements on an unbonded post-tensioned precast frame similar to those imposed on other systems by the NEHRP provisions.[8]

Yield Limit State Criteria— The yield limit is related to the strength and deformability of the beam-column connection. The demands from the design level ground motion are compared to the yield limit to ensure that the beam-column connection has adequate strength and deformability. The yield limit criteria are defined in terms of both moment and rotation. The criterion for moment is similar to the flexural strength design criterion for cast-in-place reinforced concrete. This criterion requires the beam-column connection bending moment demand corresponding to the NEHRP[8] equivalent lateral forces to be less than or equal to the factored connection bending moment capacity:

$$M_{el} \le \phi M_y \qquad (3)$$

where ϕ is the flexural capacity reduction factor in accordance with the ACI 318 Code.[9]

The yield limit criterion for rotation is used to ensure sufficient elastic deformability in the connection. The yield rotation is used, so that the post-tensioning steel in the connection can remain elastic under the design level ground motion. Avoiding yield of the post-tensioning steel permits the frame to survive the design level ground motion with little or no structural damage. The criterion is:

$$\gamma_{des\text{-}loc}\,\theta_{des} \le \theta_y \qquad (4)$$

where

$\gamma_{des\text{-}loc}$ = local ductility demand factor for the design level ground motion, greater than unity

$\theta_{des} = (M_{des}/M_{el})\,\theta_{el} = R\theta_{el}$ = beam-column connection rotation for the design level of earthquake loading, estimated from θ_{el} using an equal displacement assumption

The product $\gamma_{des\text{-}loc}\theta_{des}$ is an estimate of the rotation demand on the connection under the design level ground motion. The factor $\gamma_{des\text{-}loc}$ accounts for uncertainty in the ductility demand on the beam-column connection, as discussed later.

Ultimate Limit State Criterion — The ultimate limit is used to ensure sufficient inelastic deformability in the connection. The ultimate limit criterion is established with respect to the survival level ground motion. This criterion defines the inelastic deformability required to prevent failure of the spiral confined concrete in the beam-column connections which could lead to sudden collapse of the frame. The criterion for rotation is:

$$\gamma_{sur\text{-}loc}\,\theta_{sur} \le \theta_{ult} \qquad (5)$$

where

$\gamma_{sur\text{-}loc}$ = local ductility demand factor for survival level ground motion, greater than unity

$\theta_{sur} = (M_{sur}/M_{el})\,\theta_{el} = 2.5R\,\theta_{el}$ = beam-column connection rotation for the survival level of earthquake loading, estimated from θ_{el} using an equal displacement assumption, when the intensity of the survival level ground motion is taken as 2.5 times the intensity of the design level ground motion

The product $\gamma_{sur\text{-}loc}\,\theta_{sur}$ is an estimate of the rotation demand on the connection under the survival level ground motion. The factor $\gamma_{sur\text{-}loc}$ accounts for uncertainty in the ductility demand on the beam-column connection, as discussed later.

Flexural capacity design criteria are adopted for the frame members and connections intended to remain elastic under all loading conditions.[3,4] Columns (except at their bases) and beams (except at their ends) should possess flexural strength in excess of the bending moments corresponding to the strength of the relevant beam-column connections. Similarly, shear capacity design criteria are adopted to avoid excessive shear deformations and stiffness softening due to shear.[3,4] Shear slip at the beam-column interface should be avoided by providing appropriate shear friction resistance at the interface.

DESIGN OF PROTOTYPE FRAMES

Four prototype frames were designed using the proposed design approach.[3,4] Only two frames, Frame 1 and Frame 4 are discussed in this paper. Frame 1 and Frame 4 were designed for high and moderate seismicity zones, respectively. The 1991 edition of the NEHRP provisions was used to design the prototype frames, which were designed before the 1994 edition was published in May 1995.

The frames were designed as special moment resisting frames with R equal to 8, C_d equal to 5.5, and θ_{all} equal to 1.5 percent. The frames were designed to satisfy the requirements of both the north-south frames and the east-west frames of the prototype building. Table 2 shows the main parameters that influence the base shear demand according to NEHRP.[8]

Using the proposed design approach outlined above, connections, beams, and columns are designed for both frames. The local ductility demand factors were set to unity in the design. Table 3 summarizes the beam and column cross-sectional dimensions for the two prototype frames.

PUSH-OVER ANALYSES OF PROTOTYPE FRAMES

Nonlinear push-over static analyses of the prototype frames were conducted using a triangular distribution of lateral forces, similar to the NEHRP[8] lateral force distribution. The analyses included dead load and 25 percent of the design live load as gravity loads. All frames were analyzed as north-south frames which have less gravity load than the east-west frames. These analyses are called low gravity load (LGL) cases.

Frame 4 was also analyzed as an east-west frame (as a high gravity load (HGL) case). The frames were pushed to a target roof displacement equal to 40 in. (1020 mm), which corresponds to 4.1 percent roof drift. The static analyses used both the fiber model (FM) and the spring model (SM) for the frames. These models are similar to the beam-column subassemblage models, shown in Fig. 4.

Table 4 summarizes three levels of estimated roof displacement corresponding to the elastic (reduced), design, and survival levels of earthquake loading for the FM of each prototype frame. Table 4 also shows the calculated fundamental period of the prototype frames and the period used in design based on the 1991 edition of the NEHRP provisions.[8]

Fig. 9 shows the frame base shear (V) versus roof displacement (Δ) for both the FM and the SM of Frame 1. Fig. 10 shows V versus Δ for the FM of Frame 4. The three levels of roof displacement corresponding to the elastic (reduced), design, and survival levels of earthquake loading, given in Table 4, are shown in Figs. 9 and 10. Also shown in the figures are the range of roof displacements at which yielding of columns at the base initiates, and the range of roof displacements at which yielding of the post-tensioning steel initiates, from the FM results.

Comparing the SM to the FM in Fig. 9, the SM results are in a good agreement with those of the FM. The push-over behavior of the frames is discussed in the following paragraphs, starting with comparisons of the behavior with the proposed design requirements.

Elastic Level Requirements — All the elastic level requirements are satisfied in both frames. Spalling of the concrete cover, yielding of the steel reinforcement, and softening of the beam-column connections do not occur before the elastic (reduced) level base shear (V_{el}) is reached. Therefore, the behavior is essentially linear elastic up to the elastic level base shear. In addition, the drift limits are satisfied.

Design Level Requirements — Softening of the base shear-roof displacement behavior was observed, as expected, between the elastic level and the design level. The two main sources

Table 2. Description of the two prototype frames.

	Seismic zone	Soil conditions	Period used in design
Frame 1	High seismicity ($A_a = A_v = 0.4$)	Medium soil ($S = 1.2$) (Soil type S_2)	$T = T_a = 0.82$ seconds
Frame 4	Moderate seismicity ($A_a = A_v = 0.1$)	Medium soil ($S = 1.2$) (Soil type S_2)	$T = C_a T_a = 1.38$ seconds

A_a, A_v, T_a, C_a, S, and soil types are defined in the 1991 edition of NEHRP.[8]

Table 3. Member dimensions.

Member	Frame 1	Frame 4
All columns, in. (mm)	28 x 38 (710 x 970)	22 x 26 (560 x 660)
Sixth floor (roof) beams, in. (mm)	24 x 26 (610 x 660)	16 x 20 (410 x 510)
Fourth and fifth floor beams, in. (mm)	24 x 34 (610 x 860)	16 x 24 (410 x 610)
Second and third floor beams, in. (mm)	24 x 40 (610 x 1020)	18 x 26 (460 x 660)
First floor beams, in. (mm)	24 x 42 (610 x 1070)	18 x 26 (460 x 660)

of the softening are: (1) softening of the beam-column connections after the linear limit is reached; and (2) yielding of columns at the base of the frames. Concrete cover spalling takes place at some of the beam-column connections and column bases.

The contribution of column base yielding to the softening of the frame is expected. The first-story columns were designed to behave as conventional reinforced concrete columns. They were designed to yield at the base at a bending moment close to the moment demand for the reduced level of earthquake loading (V_{el}). In the frame analytical models, the first-story columns were modeled using beam-column elements with the possibility of yielding at the base and considering axial force-moment interaction. The columns were fixed at the base in the models.

Most of the softening of the frames observed in Figs. 9 and 10 is due to the softening of the beam-column connections after the linear limit is reached. The figures show the range of roof displacements at which yielding of columns at the base initiates. The beam-column connections reach their linear limit at similar or slightly larger values of roof displacement.

A significant redistribution of internal forces (compared to the linear elastic distribution) occurs due to softening of the frame. This causes yielding of the post-tensioning steel to occur over a wide range of roof displacement values. In general, the sequence of yielding of the post-tensioning steel progresses from the lower floors to the upper floors.

According to the yield limit state design criteria, yielding of the post-tensioning steel should not occur before the design level roof displacement (Δ_{des}) is reached. This criterion is not satisfied for Frame 1 (designed for high seismicity regions), but is satisfied for Frame 4 (designed for moderate seismicity regions). As discussed earlier, local ductility demand factors ($\gamma_{des\text{-}loc}$) are needed to amplify the design ductility demands on the beam-column connections, so that under the design level ground motions the post-tensioning steel will not yield before the design level roof displacement

Table 4. Roof displacements estimated in design and fundamental periods based on the fiber model.

Parameter	Frame 1	Frame 4
Δ_{el}, in. (mm)	1.62 (41)	1.38 (35)
Δ_{des}, in. (mm)	13.0 (330)	11.0 (279)
Δ_{sur}, in. (mm)	32.4 (823)	27.6 (701)
T	1.12 seconds	2.48 seconds
T used in design	0.82 seconds	1.38 seconds

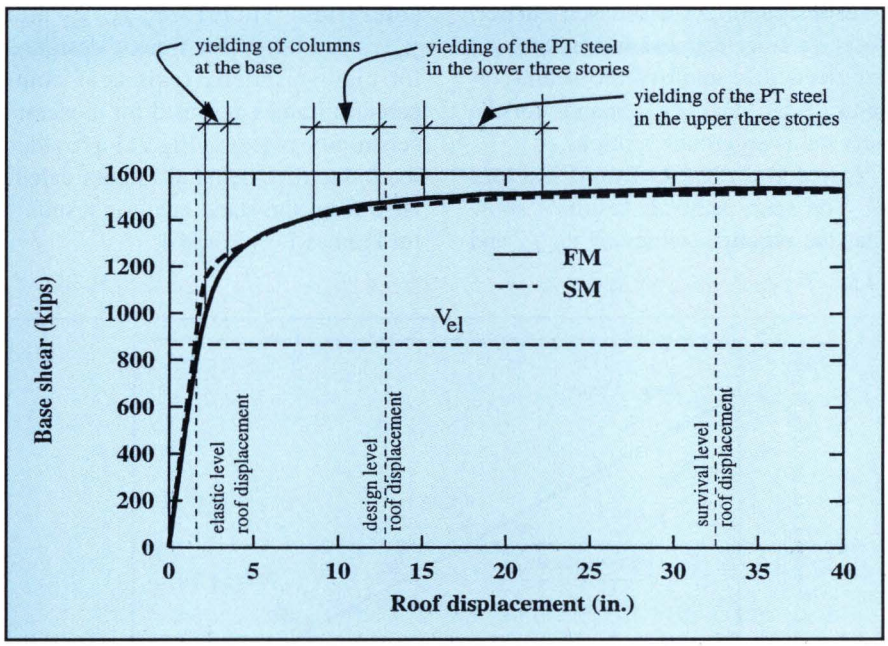

Fig. 9. Base shear vs. roof displacement of Frame 1, using the FM and the SM.
Note: 1 in. = 25.4 mm; 1 kip = 4.45 kN.

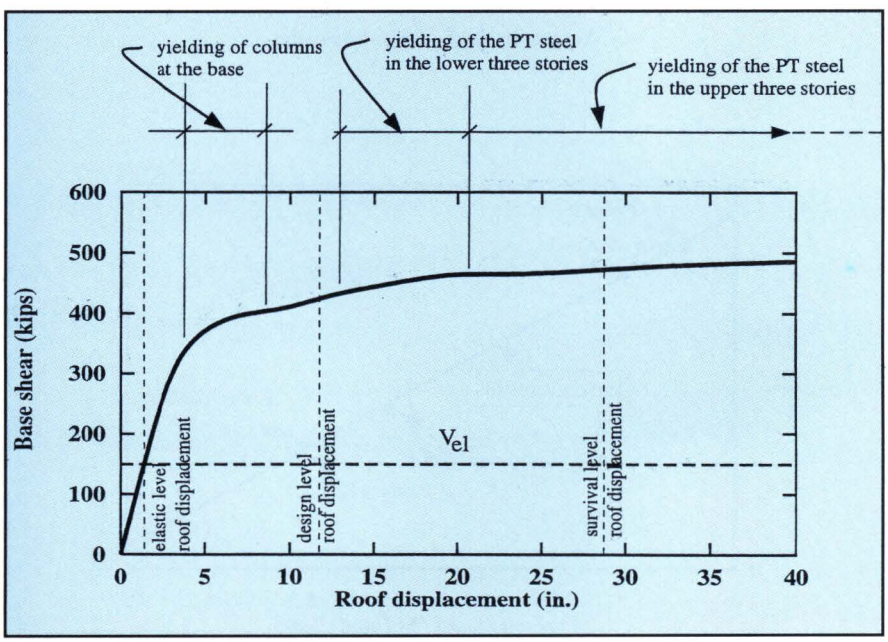

Fig. 10. Base shear vs. roof displacement of Frame 4, using the FM.
Note: 1 in. = 25.4 mm; 1 kip = 4.45 kN.

(Δ_{des}) is reached. Local ductility demand factors are discussed below.

Survival Level Requirements — According to the ultimate limit state design criterion, up to the survival level roof displacement, the confined concrete strain should not exceed the ultimate strain for the confined concrete (ε_{cu}) to avoid failure of concrete due to fracture of the spiral confining steel in the beam-column connections. The prototype frames did not experience this type of failure because the spirals in the prototype frames were overdesigned. As discussed earlier, local ductility demand factors ($\gamma_{sur\text{-}loc}$) are needed to amplify the beam-column design ductility demands for the survival level ground motions.

Local Ductility Demand Factors — The static analysis results[3,4] show that the required values of $\gamma_{des\text{-}loc}$ and $\gamma_{sur\text{-}loc}$ decrease as the contribution of gravity load to the beam-column connection design moment demand increases. The gravity load contribution to the design moment leads to an overdesign of the moment capacity of the beam-column connection that reduces the ductility demand. The gravity load contribution can be estimated as the ratio between the bending moment demand due to gravity loads and the total elastic bending moment demand including both gravity and lateral loads at the connection under consideration. Therefore, $\gamma_{des\text{-}loc}$ and $\gamma_{sur\text{-}loc}$ are larger for frames designed for high seismicity regions as compared to frames designed for moderate seismicity regions. Fig. 11 provides local ductility demand factors calculated from the static analysis results[3,4] for Frames 1, 2, 3, and 4.

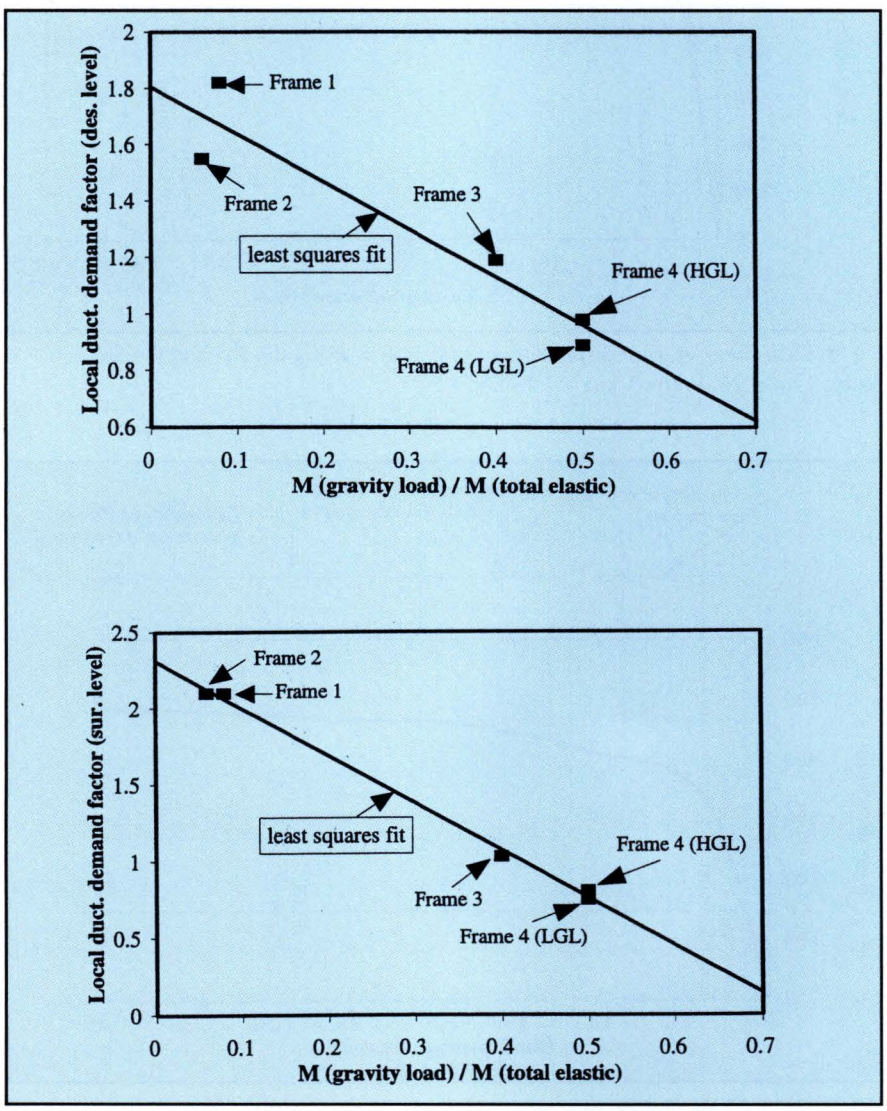

Fig. 11. Local ductility demand factors for design and survival ground motions.

Beam Elongation — One of the issues to be considered in the design of an unbonded post-tensioned precast concrete frame is the apparent elongation of the beams due to gap opening in the beam-column connections. As the lateral drift of the frame increases, the gap opening length and width increase at the beam-column interface and, accordingly, the centroidal axis of the beam measured from column face to column face elongates. The FM was used to study the beam elongation, and for the prototype frames the elongation was found to range between 1.5 to 2.5 percent of the beam height (h), for each beam span (L_b), as the roof drift reached 4.0 percent.

Two factors affect the elongation of the beams: foundation restraint on the columns; and relative beam elongations between adjacent floors. The effect of the foundation restraint is dominant for the lower floor beams. The effect of relative beam elongations between adjacent floors is not easily predicted.

The restraint of the beam elongation in the frame introduces a set of self-equilibrating forces in the frame, including forces at the foundation level. The beam-column connections and beams are subjected to additional axial forces, while the columns are subjected to secondary shear forces and bending moments. The axial forces in the beams are usually maximum at the first floor. The secondary shears and moments in the columns are proportional to their distance from the column at the center of the frame.

The effect of these axial forces in the beams is as follows: (1) the axial compression forces increase the bending moment capacity, increase the yield rotation, and decrease the ultimate rotation of the beam-column connections; and (2) the axial tension forces decrease the bending moment capacity, decrease the yield rotation, and increase ultimate rotation of the beam-column connections. The beam elongation effects should be considered in design. For example, the increase in the beam-column connection bending moment capacity was observed to be as large as 25 percent.

TIME-HISTORY DYNAMIC ANALYSES OF FRAME 1

The results of nonlinear time-history dynamic analyses of prototype Frame 1 are described in this section. The frame is analyzed for design and survival level earthquake ground motions. Natural recorded and artificially generated ground motions for different soil conditions (stiff/rock, medium, and soft soil) were used in the dynamic analyses. Table 5 summarizes the main characteristics of these ground motions, scaled to a peak ground acceleration (PGA) of 1.0*g*. Damping of the prototype frames is modeled as mass and stiffness proportional viscous damping, with a specified damping ratio of 3.0 percent for the first and third modes, and resulting damping ratios of 2.2 percent for the second mode, and 4.3 percent for the fourth mode.

Roof Displacement — The roof lateral displacement is representative of the overall frame displacement response. Fig. 12 shows time-histories of the lateral displacement of the roof and the second and fourth floor levels of Frame 1 during the NEW ground motion scaled to a peak ground acceleration of 0.4*g* to represent a design level ground motion. The dashed horizontal lines shown in Fig. 12 indicate the roof displacement for the design level ground motion estimated in design (Table 4). Fig. 12 shows that the roof displacement obtained from the dynamic analysis does not exceed the roof displacement estimated in design. Fig. 12 also shows that, at the time of the displacement peaks, the second and fourth floor displacements are generally in phase with the roof displacements.

Maximum Roof Displacement — The maximum roof displacement values obtained from the dynamic analyses of Frame 1 are tabulated in Table 6, where the corresponding roof drift values (the roof displacement divided by the total frame height) are also given. Fig. 13 compares the roof displacements obtained from the dynamic analyses (shown as discrete points), and the estimated roof displacements based on an equal displacement assumption (shown as an inclined solid line). The roof displacements are shown as a function of peak ground acceleration (PGA). Three symbols represent the dynamic analysis results for the three soil conditions (stiff/rock, medium, and soft soil).

Table 5. Properties of selected ground motions scaled to 1.0*g*.

Site soil condition	Earthquake		Earthquake/station name (year)	Peak ground acceleration (*g*)	Peak ground velocity (in./second)
	No.	Record			
Rock or stiff	1	ELC	El Centro/El Centro (1940)	1.00	43.6
	2	PRE	Loma Prieta/Presidio (1989)	1.00	66.3
	3	GST	Power spectrum based generated ground motion	1.00	77.8
	4	STF	SEAOC spectrum compatible generated ground motion	1.00	60.6
Medium	5	ORI	San Fernando/Orion (1971)	1.00	45.9
	6	HOL	Loma Prieta/Hollister (1989)	1.00	67.4
	7	YER	Landers/Yermo (1992)	1.00	82.5
	8	NEW	Northridge/Newhall (1994)	1.00	64.0
	9	SYL	Northridge/Sylmar (1994)	1.00	60.4
	10	GME	Power spectrum based generated ground motion	1.00	104
	11	MED	SEAOC spectrum compatible generated ground motion	1.00	107
Soft	12	FOS	Loma Prieta/Foster City (1989)	1.00	62.8
	13	TRE	Loma Prieta/Treasure Island (1989)	1.00	82.3
	14	GSO	Power spectrum based generated ground motion	1.00	147
	15	SOF	SEAOC spectrum compatible generated ground motion	1.00	80.4

Note: 1 in. = 25.4 mm.

As shown in Fig. 13, all of the roof displacements from the dynamic analyses for cases with stiff/rock soil conditions are conservatively estimated using the equal displacement assumption. For cases with medium soil conditions, the average of the roof displacements from the dynamic analyses are conservatively estimated. All of the roof displacements from dynamic analysis for cases with soft soil conditions exceed the estimated roof displacements.

Implications for Design — Fig. 13 shows that the maximum roof displacement values obtained from the dynamic analyses often exceed the estimated roof displacements, especially for design level ground motions on soft soil conditions and survival level ground motions on medium or soft soil conditions. When the estimated roof displacements are exceeded, the ductility demands on beam-column connections are larger than expected, and adequate ductility capacity may not be available. Moreover, the maximum roof displacements during survival level ground motions on medium and soft soil conditions are unacceptably large.

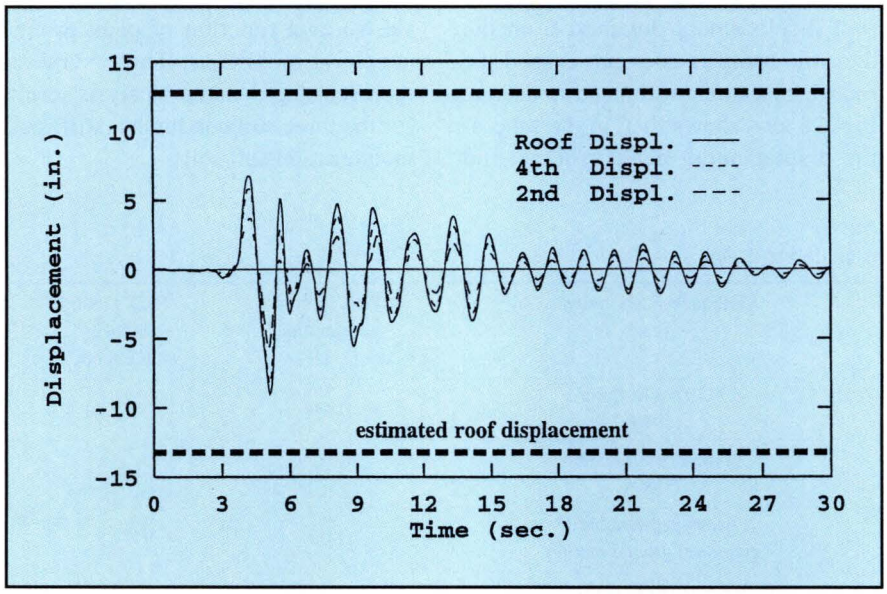

Fig. 12. Displacement time-histories of Frame 1 during NEW ground motion scaled to a peak ground acceleration of 0.4*g*. **Note:** 1 in. = 25.4 mm.

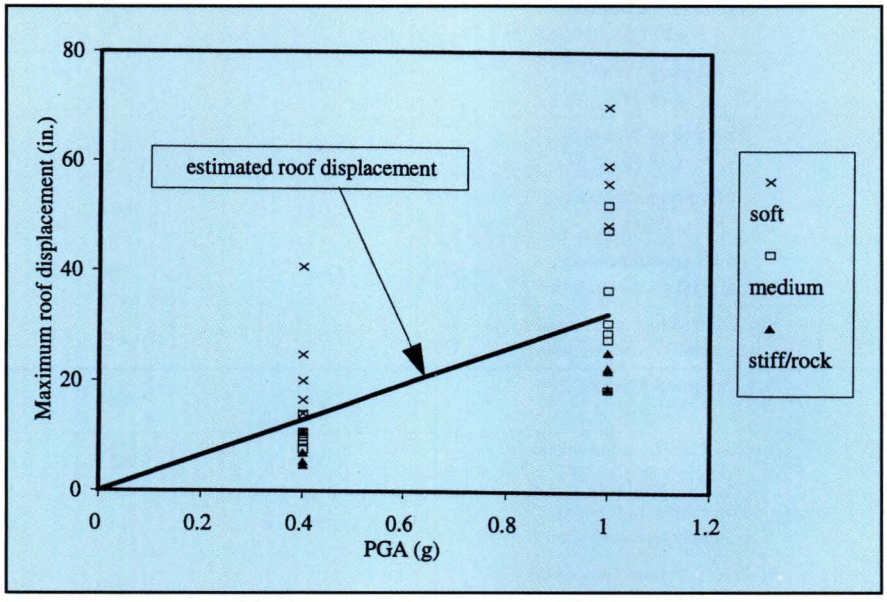

Fig. 13. Maximum roof displacement of Frame 1 vs. peak ground acceleration (PGA) of the ground motion. **Note:** 1 in. = 25.4 mm.

It should be kept in mind that the estimated roof displacements are based on elastic analysis under NEHRP[8] equivalent lateral forces for medium soil and 5 percent damping. The estimated displacements are based on the approximate period given by the 1991 edition of the NEHRP provisions[8] which is smaller than the actual period of Frame 1, as indicated in Table 4. An improved design approach would estimate the roof displacement demands using a NEHRP design spectra for the proper damping ratio, actual soil condition, and actual period of the frame.

Displacement amplification factors, similar to load factors, can be developed on a probabilistic basis to scale up the estimated roof displacements to account for the observed scatter in the displacements from dynamic analyses. These displacement amplification factors should depend on the seismic zone and the soil conditions of the building site. Suggested values of the displacement amplification factors are given in reports by El-Sheikh et al.[3,4]

Using these displacement amplification factors, Frame 1 could be redesigned to: (1) decrease the maximum roof displacement (e.g., by increasing the stiffness) during the survival level ground motions on medium and soft soil conditions to an acceptable level (e.g., 3.0 percent roof drift to prevent failure of the gravity load resisting system and maintain structural integrity); and (2) provide sufficient ductility capacities to the beam-column connections to satisfy the ductility demands.

Base Shear — Fig. 14 shows the base shear of Frame 1 during the NEW ground motion scaled to a peak ground acceleration of 1.0*g*. The dashed horizontal lines indicate the static base shear capacity of the frame obtained from push-over analysis under the inertia force distribution specified in the NEHRP[8] equivalent lateral forces procedure. The peak values of base shear reached during the dynamic analysis are significantly larger than the static base shear capacity, primarily because of the contribution of higher modes.

Effect of Inelastic Energy Dissipation and Self-Centering — The

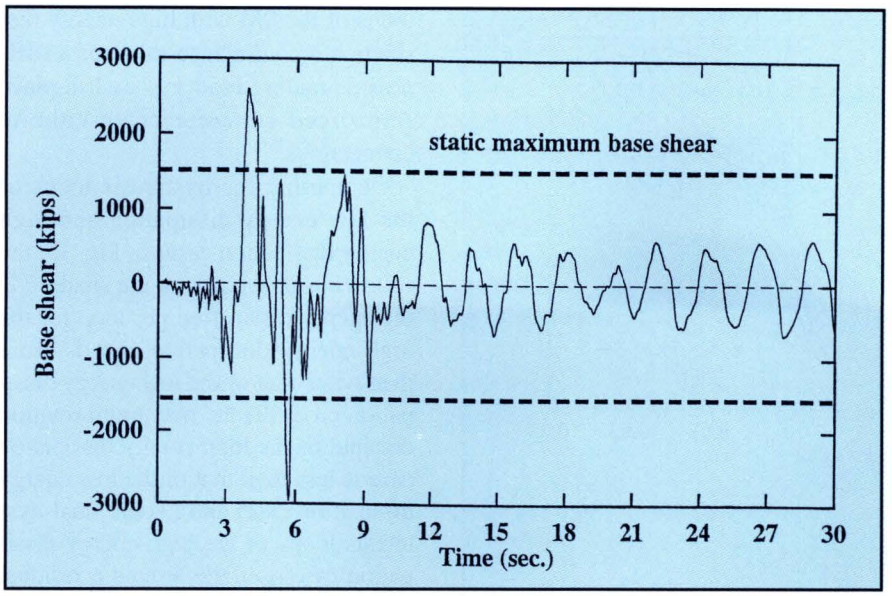

Fig. 14. Base shear time-history of Frame 1 during NEW ground motion scaled to a peak ground acceleration of 1.0*g*. **Note:** 1 kip = 4.45 kN.

effect of the inelastic energy dissipation and self-centering provided by unbonded post-tensioned precast concrete frames were investigated. The SM was used because the beam-column connection hysteresis behavior can be directly controlled by specifying different residual deformation factors (α_r).[3,4] Increases in α_r increase the energy dissipated by the beam-column connections and decrease the self-centering. Frame 1 was investigated using TRE ground motion scaled to a peak ground acceleration of 0.4*g*. Two α_r values (0.03 and 0.90) were considered.

The SM with the small α_r tends to have low energy dissipation (LED) and represents an unbonded post-tensioned precast concrete frame. The SM with the large α_r tends to have high energy dissipation (HED) and represents a conventional cast-in-place reinforced concrete frame. Fig. 15(a) shows the moment-rotation behavior of one of the first floor beam-column connections of Frame 1 modeled with the FM and the SM with low energy dissipation (LED). Fig. 15(b) shows the moment-rotation behavior of the same connection modeled with the SM with high energy dissipation (HED).

Fig. 15(a) shows a relatively good comparison between the FM and the SM with low energy dissipation, however, the increase in bending moment capacity of the beam-column connection due to the axial compression force in the first floor beams is captured only by the FM. The hysteresis

Table 6. Maximum seismic response parameters of Frame 1.

Peak ground acceleration	Soil type	Ground motion	Maximum roof displacement (in.)	Maximum roof drift (percent)	Maximum story drift (percent)	Maximum base shear (kips)
0.4*g* design level	Stiff/Rock	ELC	5.33	0.55	0.72	1378
		PRE	10.74	1.11	1.51	1795
		STF	4.74	0.49	0.87	1595
		GST	6.92	0.71	1.30	1686
	Medium	SYL	10.68	1.10	1.67	2043
		HOL	9.73	1.00	1.76	1850
		YER	13.90	1.43	1.95	1760
		ORI	10.35	1.07	1.83	1846
		NEW	9.01	0.93	1.80	2024
		MED	9.84	1.01	1.68	1757
		GME	7.53	0.78	1.30	1730
	Soft	TRE	24.74	2.55	3.46	2000
		FOS	16.55	1.70	2.47	1923
		SOF	19.98	2.06	3.31	2190
		GSO	14.11	1.45	2.19	2165
1.0*g* survival level	Stiff/Rock	ELC	22.14	2.28	2.80	2230
		PRE	18.90	1.94	3.58	2641
		STF	25.41	2.61	3.87	2757
		GST	22.60	2.33	3.41	2305
	Medium	SYL	27.71	2.85	3.75	2535
		HOL	52.26	5.38	6.42	2727
		YER	18.59	1.91	2.97	2433
		ORI	30.75	3.16	4.41	2388
		NEW	29.04	2.99	4.11	2957
		MED	36.72	3.78	5.69	2797
		GME	47.67	4.90	5.84	2716
	Soft	TRE	56.19	5.78	6.14	3000
		FOS	48.56	5.00	5.65	2716
		SOF	59.37	6.11	7.32	3122
		GSO	70.12	7.21	7.96	3063

Note: 1 in. = 25.4 mm; 1 kip = 4.45 kN.

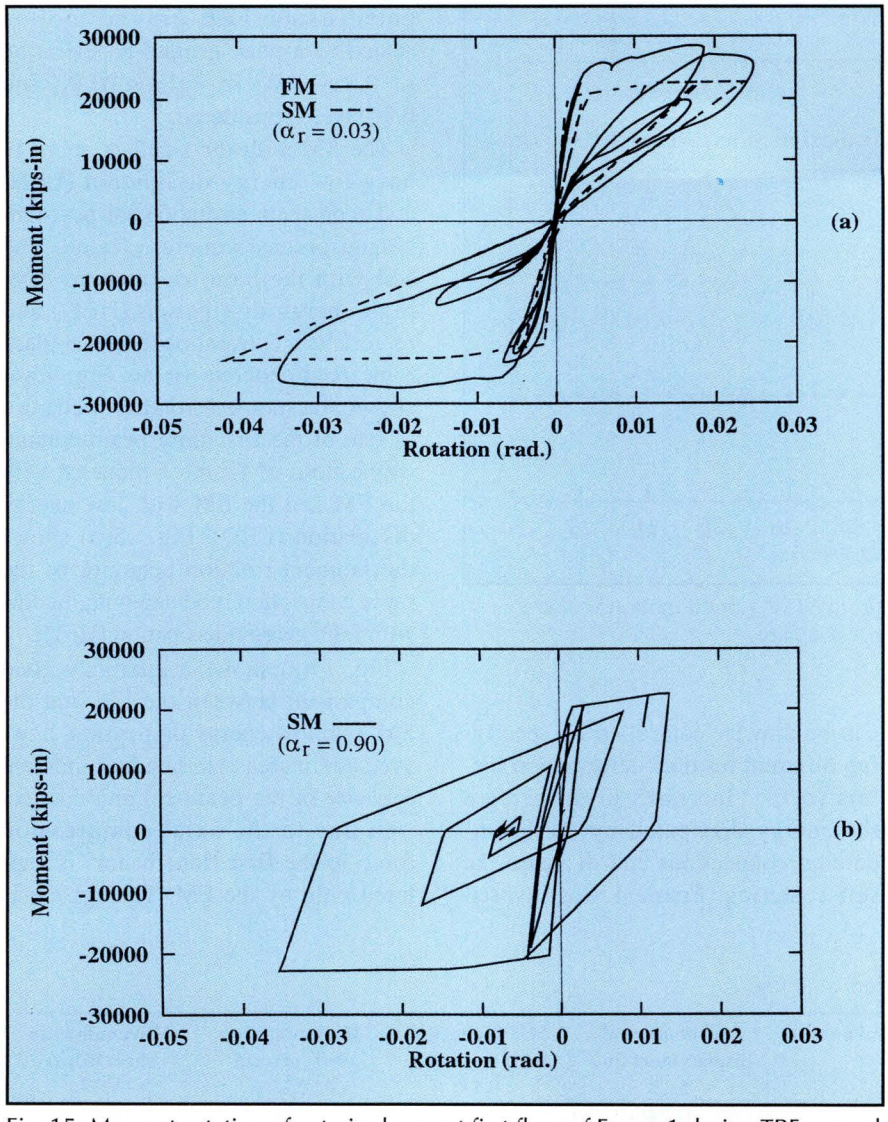

Fig. 15. Moment-rotation of exterior beam at first floor of Frame 1 during TRE ground motion scaled to a peak ground acceleration of 0.4*g*: (a) using the FM and the SM with low energy dissipation; (b) using the SM with high energy dissipation. **Note:** 1 in. = 25.4 mm; 1 kip = 4.45 kN.

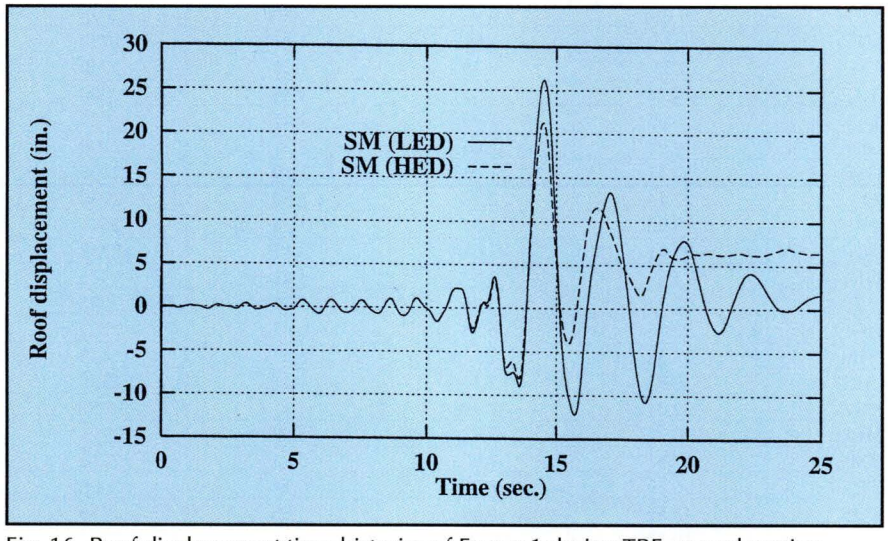

Fig. 16. Roof displacement time-histories of Frame 1 during TRE ground motion scaled to a peak ground acceleration of 0.4*g*, using the SM with low energy dissipation (LED) and high energy dissipation (HED). **Note:** 1 in. = 25.4 mm.

loops of the SM with high energy dissipation are similar to those of a stiffness-degrading model of cast-in-place reinforced concrete beam-column connections.

Comparing the hysteresis loops of the low energy dissipation and high energy dissipation cases in Fig. 15, the following observations are made: (1) the energy dissipation per loop for the high energy dissipation case is more than twice that of the low energy dissipation case; (2) the maximum rotation demand of the high energy dissipation case is less than that of the low energy dissipation case; and (3) the final hysteresis loops of the high energy dissipation case oscillate around a residual rotation, while all loops of the low energy dissipation case oscillate around zero rotation.

Fig. 16 shows roof displacement time-histories for the SM of Frame 1 with low energy dissipation and high energy dissipation during the 0.4*g* TRE ground motion. The maximum roof displacement for the high energy dissipation case is smaller than that of the low energy dissipation case by about 19 percent. The amplitude of the displacement cycles following the maximum displacement decays more rapidly for the high energy dissipation case. The low energy dissipation case has several successive large displacement cycles. On the other hand, the low energy dissipation case has self-centering (i.e., the roof displacement oscillates around zero displacement), which results in a small residual displacement.

TIME-HISTORY DYNAMIC ANALYSES OF FRAME 4

The dynamic analyses of Frame 4 show the frame performs well and satisfies the design criteria. The maximum roof displacements are significantly less than the roof displacement estimated in design. Two factors should be noted: (1) the large difference between the maximum period allowed in the NEHRP[8] design procedure (C_aT_a = 1.38 seconds) and the actual period of the frame (T = 2.48 seconds), and (2) the large contribution of the gravity load moment to the moment used to design the beam-column connections.

Table 7. Maximum seismic response parameters of Frame 4 during the TRE ground motion.

Peak ground acceleration	Maximum roof displacement (in.)	Maximum roof drift (percent)	Maximum story drift (percent)	Maximum base shear (kips)
0.1*g* design level	8.86	0.91	1.24	481
0.25*g* design level	14.6	1.51	1.97	623

Note: 1 in. = 25.4 mm; 1 kip = 4.45 kN.

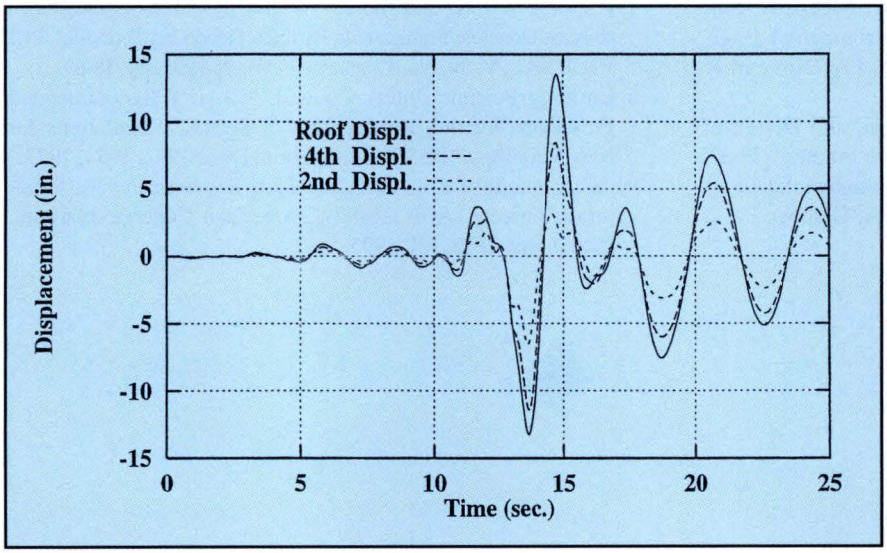

Fig. 17. Displacement time-histories of Frame 4 during TRE ground motion scaled to a peak ground acceleration of 0.25*g*. **Note:** 1 in. = 25.4 mm.

Both factors result in a significant overstrength of the base shear of the frame above the base shear used in design (V_{el}), as shown in Fig. 10. Consequently, the ductility demands are significantly less than those of Frame 1. Table 7 summarizes the dynamic response of Frame 4 during the TRE ground motion scaled to a peak ground acceleration of 0.1*g* and 0.25*g* to represent the design and the survival level ground motions, respectively. Fig. 17 shows time-histories of the lateral displacement of the roof and the second and fourth floor levels of Frame 4 during the TRE ground motion scaled to a peak ground acceleration of 0.25*g*. The maximum roof drift reaches only 1.5 percent.

CONCLUSIONS

Based on the research findings presented in this paper, the following conclusions are drawn:

1. For design, the moment-rotation behavior of a beam-column connection can be represented by a trilinear idealization developed using approximate formulas for three limit states in the behavior.

2. Unbonded post-tensioned precast frames can be designed using the design approach described in this paper. However, the design criteria should not be based on the displacements estimated using an equal displacement assumption for frames on medium or soft soil conditions in regions of high seismicity. Displacement amplification factors similar to those given in reports by El-Sheikh et al.[3,4] should be used under these conditions.

3. Local ductility demand factors (γ-factors) are needed to amplify the local ductility demands for the beam-column connections. The local ductility demand factors are larger for frames designed for high seismicity regions than for frames designed for moderate seismicity regions.

4. Compared to similar cast-in-place reinforced concrete frames, the maximum displacement of unbonded post-tensioned precast frames under seismic loading is expected to be larger, due to the small energy dissipation, while the accumulated residual displacement is expected to be much smaller.

ACKNOWLEDGMENTS

This investigation was funded by the National Science Foundation (NSF) under Grant No. BCS-9307880 as part of the Precast Seismic Structural Systems (PRESSS) research program. The support of the NSF Program Director, Dr. S. C. Liu and Program Coordinator Dr. M. J. N. Priestley is gratefully acknowledged. Financial support for the first author was provided by Cairo University, Egypt.

The investigation was carried out at the center for Advanced Technology for Large Structural Systems (ATLSS) at Lehigh University. The authors wish to thank the reviewers for their thoughtful comments. The opinions, findings, and conclusions expressed in this paper are those of the authors.

REFERENCES

1. Priestley, M. J. N., "Overview of PRESSS Research Program," PCI JOURNAL, V. 36, No. 4, July-August 1991, pp. 50-57.
2. Nakaki, S., and Englekirk, R., "PRESSS Industry Seismic Workshops: Concept Development," PCI JOURNAL, V. 36, No. 5, September-October 1991, pp. 54-61.
3. El-Sheikh, M., Pessiki, S., Sause, R., Lu, L.-W., and Kurama, Y., "Seismic Analysis, Behavior, and Design of Unbonded Post-Tensioned Precast Concrete Frames," Earthquake Engineering Research Report, Report No. EQ-97-02, Department of Civil and Environmental Engineering, Lehigh University, Bethlehem, PA, November 1997.
4. El-Sheikh, M., "Seismic Analysis, Behavior, and Design of Unbonded Post-Tensioned Precast Concrete Frames," Ph.D. Dissertation, Department of Civil and Environmental Engineering, Lehigh University, Bethlehem, PA, October 1997, 456 pp.
5. Prakash, V., Powell, G., and Campbell, S., "DRAIN-2DX Base Program Description and User Guide; Version 1.10," Report No. UCB/SEMM-93/17&18, Structural Engineering Mechanics and Materials, Department of Civil Engineering, University of California, Berkeley, CA, December 1993.
6. Cheok, G., and Lew, H. S., "Model Precast Concrete Beam-to-Column Connections Subject to Cyclic Loading," PCI JOURNAL, V. 38, No. 4, July-August 1993, pp. 80-92.
7. Priestley, M. J. N., and Tao, J., "Seismic Response of Precast Prestressed Concrete Frames with Partially Debonded Tendons," PCI JOURNAL, V. 38, No. 1, January-February 1993, pp. 58-69.
8. Building Seismic Safety Council, "NEHRP Recommended Provisions for the Development of Seismic Regulations for New Buildings," BSSC, Washington, D.C., 1991, 1994, 1997.
9. ACI Committee 318, "Building Code Requirements for Structural Concrete (ACI 318-95)," American Concrete Institute, Farmington Hills, MI, 1995.

APPENDIX — NOTATION

a = compression stress block depth
a'' = compression stress block depth, measured from inside spirals, when spiral confined concrete fails
A_p = total cross-sectional area of post-tensioning steel
b = beam cross-sectional width
b'' = beam cross-sectional width, measured from inside spirals
c'' = neutral axis depth, measured from inside spirals, when spiral confined concrete fails
C_a = period modification factor defined in NEHRP
C_d = inelastic deflection amplification factor defined in NEHRP
$c_l = f_{pl}/f_{pu}$
E_c = concrete Young's modulus of elasticity
E_p = post-tensioning steel Young's modulus of elasticity
f_c' = maximum compressive strength of unconfined concrete
f_{cc}' = maximum compressive strength of confined concrete
f_{ci} = concrete initial stress
f_{pi} = post-tensioning steel initial stress
f_{pl} = post-tensioning steel stress at its limit of proportionality (post-tensioning steel yield stress)
f_{pu} = post-tensioning steel ultimate strength
h = total height of beam
h'' = confined beam height, measured from inside spirals
L_b = beam span between inflection points
L_{bc} = beam clear length between column faces
L_{cr} = failure (crushing) length of spiral confined concrete, adjacent to beam-column interface
L_{pu} = total unbonded length of post-tensioning steel for exterior beam-column connections or half the unbonded length of post-tensioning steel for interior beam-column connections
M_{dec} = beam decompression moment (at decompression limit state)
M_{des} = beam-column connection moment for design level of earthquake loading
M_{el} = beam-column connection moment demand for reduced level of earthquake loading
M_{ll} = beam linear limit moment (at linear limit state)
M_{sur} = beam-column connection moment for survival level of earthquake loading
M_{ult} = beam ultimate moment (at ultimate limit state)
M_y = beam yield moment (at yield limit state)
R = response modification factor defined in NEHRP
T = building fundamental period
T_a = approximate period defined in NEHRP
V_{des} = design base shear
V_{el} = elastic base shear corresponding to reduced level of earthquake loading
V_{ll} = base shear at effective linear limit state
V_{sur} = survival base shear
V_{ult} = base shear at ultimate limit state
V_y = base shear at yield limit state
α = equivalent stress block coefficient for confined concrete equal to ratio of stress of stress block to maximum compressive strength of concrete
α_r = residual deformation factor
β = equivalent stress block coefficient for confined concrete equal to ratio of stress block depth to neutral axis depth
$\gamma_{des\text{-}loc}$ = local ductility demand factor for design level ground motion
$\gamma_{sur\text{-}loc}$ = local ductility demand factor for survival level ground motion
Δ_{des} = roof displacement for design level of earthquake loading
Δ_{el} = roof displacement corresponding to elastic (reduced) level of earthquake loading
Δ_{ll} = roof displacement at effective linear limit state
Δ_{sur} = roof displacement for survival level of earthquake loading
Δ_{ult} = roof displacement at ultimate limit state
Δ_y = roof displacement at yield limit state
ε_{cu} = ultimate compression strain of spiral confined concrete
θ_{all} = allowable rotation which is taken as inelastic story drift of NEHRP provisions
θ_{des} = beam-column connection rotation for design level of earthquake loading
θ_{el} = beam-column connection rotation demand for reduced level of earthquake loading
θ_{ll} = beam linear limit rotation (at linear limit state)
θ_{sur} = beam-column connection rotation for survival level of earthquake loading
θ_{ult} = beam ultimate rotation (at ultimate limit state)
θ_y = beam yield rotation (at yield limit state)
ϕ = capacity reduction factor

Seismic Behavior and Design of Unbonded Post-Tensioned Precast Concrete Walls

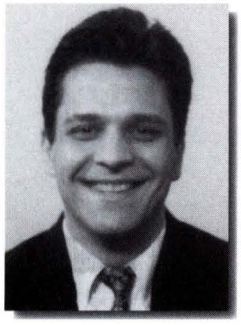

Yahya Kurama, Ph.D.
Assistant Professor
Department of Civil Engineering and Geological Sciences
University of Notre Dame
Notre Dame, Indiana

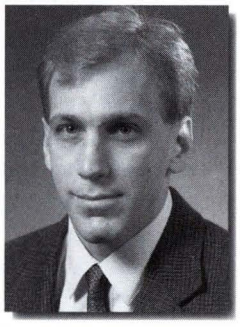

Stephen Pessiki, Ph.D.
Associate Professor
Department of Civil and Environmental Engineering
Lehigh University
Bethlehem, Pennsylvania

Richard Sause, Ph.D., P.E.
Associate Professor
Department of Civil and Environmental Engineering
Lehigh University
Bethlehem, Pennsylvania

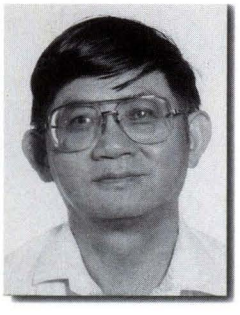

Le-Wu Lu, Ph.D.
Professor
Department of Civil and Environmental Engineering
Lehigh University
Bethlehem, Pennsylvania

Unbonded post-tensioned precast concrete walls are constructed by post-tensioning precast wall panels across horizontal joints using post-tensioning steel which is not bonded to the concrete. This paper describes an analytical investigation of the seismic behavior and design of these walls. Unbonded post-tensioned precast walls with strength and initial stiffness similar to monolithic cast-in-place concrete walls can be designed to soften and undergo large nonlinear lateral drift with little damage. The nonlinear behavior is primarily due to the opening of gaps along the horizontal joints. A performance-based seismic design approach is proposed in which the walls are required to resist design level ground motions with little damage and severe survival level ground motions with damage but without failure. Shear slip along the horizontal joints is prevented by design. Nonlinear dynamic analyses show that, compared to cast-in-place walls, unbonded post-tensioned precast walls undergo larger drift, but accumulate significantly smaller residual drift during an earthquake.

The use of precast concrete walls as primary lateral load resisting systems in seismic regions is constrained by current building codes in the United States, which require that these walls emulate the behavior of monolithic cast-in-place reinforced concrete walls. However, field studies after previous earthquakes and experimental evidence[1-3] have revealed that significant damage occurs in precast walls which emulate cast-in-place walls. Moreover, precast walls which emulate cast-in-place walls do not have all of the economic advantages of precast con-

crete construction due to the use of steel and/or cast-in-place concrete components in their joints. This paper summarizes recent research at Lehigh University on the use of unbonded post-tensioned precast walls as a primary lateral load resisting system in high and moderate seismic regions.

Unbonded post-tensioned precast walls are constructed by post-tensioning precast wall panels across horizontal joints at the floor levels using post-tensioning steel which is not bonded to the concrete (Fig. 1). Dry-pack or grout may be used between the panels for alignment and for construction tolerances. These walls do not emulate the behavior of cast-in-place concrete walls. The lateral load resistance is provided by high-strength post-tensioning steel bars or multi-strand tendons, located inside ducts which are not grouted. Spiral reinforcing steel is used to confine the concrete in the wall panels near the base of the wall. Wire mesh is used as bonded reinforcement in the panels.

The research summarized in this paper is part of the PREcast Seismic Structural Systems (PRESSS) research program.[4] The research, presented in more detail by Kurama et al.,[5,6] has the ultimate goal of developing seismic building code specifications for precast walls comparable to specifications available for cast-in-place walls.

This paper shows that unbonded post-tensioned precast walls offer many significant advantages as primary lateral load resisting systems without emulating cast-in-place concrete walls, and proposes a performance-based seismic design approach for the walls. The proposed design approach can be easily incorporated into current seismic building code specifications.

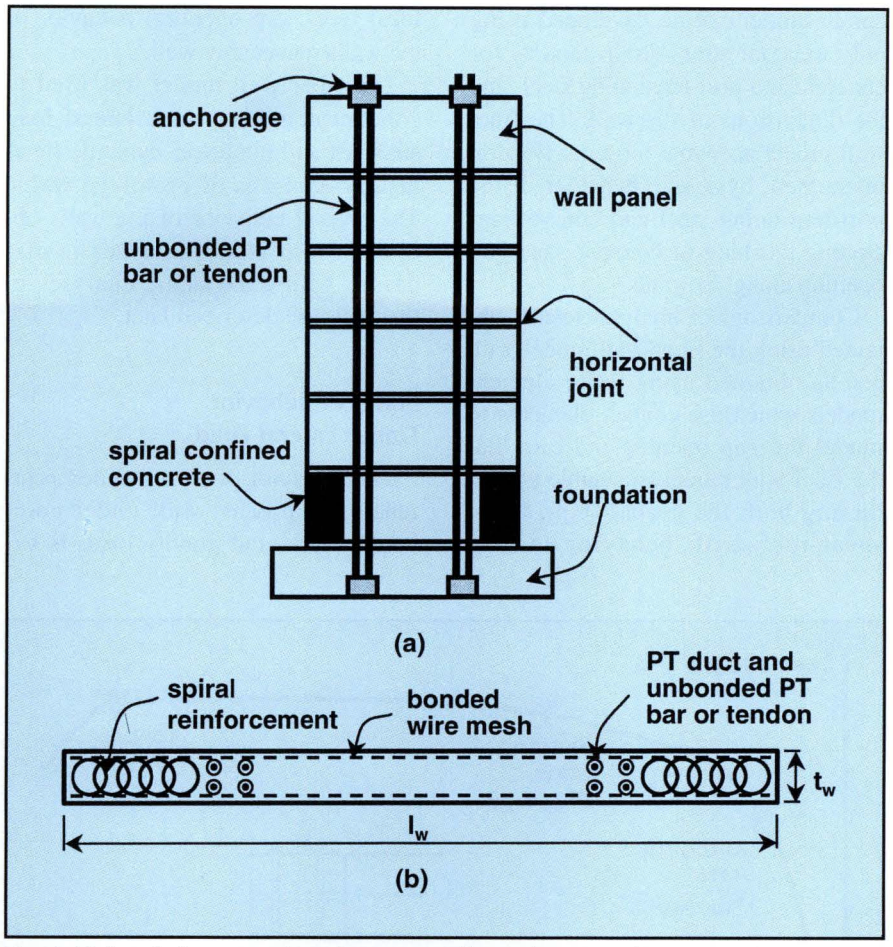

Fig. 1. Unbonded post-tensioned precast wall: (a) elevation; (b) cross section near base (enlarged).

BEHAVIOR UNDER LATERAL LOAD

The behavior of an unbonded post-tensioned precast wall under lateral load is governed by the behavior along the horizontal joints. Fig. 2 shows the two types of behavior that can occur along the joints, namely, gap opening and shear slip. In the case of gap opening, the post-tensioning force and the axial force due to gravity load provide a restoring force that tends to close the gaps upon unloading.

In the case of shear slip, however, there is no restoring force to reverse the slip. Thus, it is difficult to control the magnitude of the shear slip displacements which may occur during an earthquake. Shear slip should be prevented by proper design and detailing of the wall.

An analytical model based on fiber beam-column elements was developed to investigate the behavior of walls which are designed to have a gap opening along the joints but not shear slip.[5] A significant advantage of using fiber elements is that a reasonably ac-

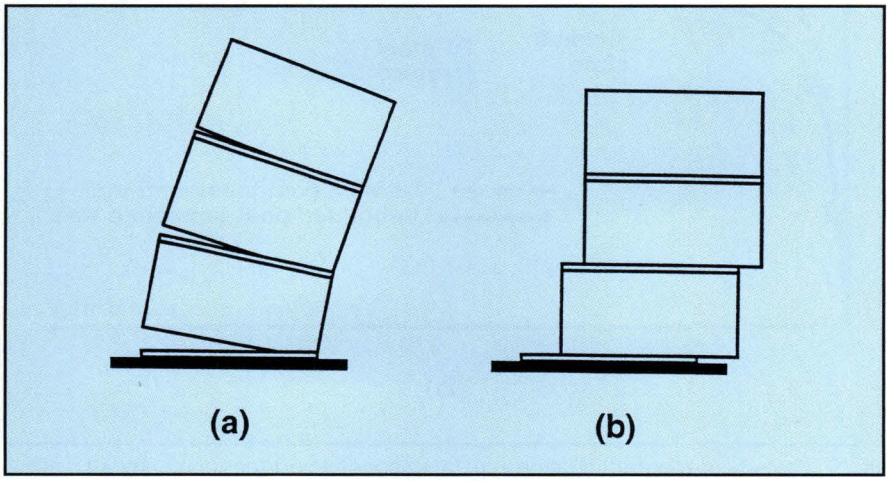

Fig. 2. Behavior of wall along horizontal joints: (a) gap opening; (b) shear slip.

curate model can be developed using only uniaxial stress-strain models for concrete and post-tensioning steel, and the dimensions of the wall. The fiber wall model accounts for axial-flexural interaction, hysteretic behavior of the post-tensioning steel and concrete including crushing of concrete, and gap opening along the joints.

Comparisons of analysis results obtained using the fiber wall model with results obtained using finite element models which use contact elements to model the gap opening indicate that the fiber wall model is capable of predicting both the global (e.g., base-shear-roof-drift) behavior and the local (e.g., gap opening) behavior of the walls reasonably well.[7]

The fiber wall model was used to conduct nonlinear static lateral load analyses and nonlinear dynamic time-history analyses of prototype walls. The typical behavior of the walls obtained from static analyses is discussed below. Dynamic analyses of the walls are described later.

States of Behavior Under Lateral Load

The behavior of an unbonded post-tensioned precast wall under combined lateral and gravity loads is explored using the base-shear-roof-drift relationship shown in Fig. 3(a). The base-shear-roof-drift relationship of a properly designed wall is governed by axial-flexural behavior (i.e., behavior under combined axial force and flexure). Shear slip behavior should not occur. The base shear, V, is equal to the sum of the lateral loads applied at the floor and roof levels, and the roof drift, Δ, is equal to the roof lateral displacement divided by the wall height. As the wall displaces, it goes through four states which are described below.

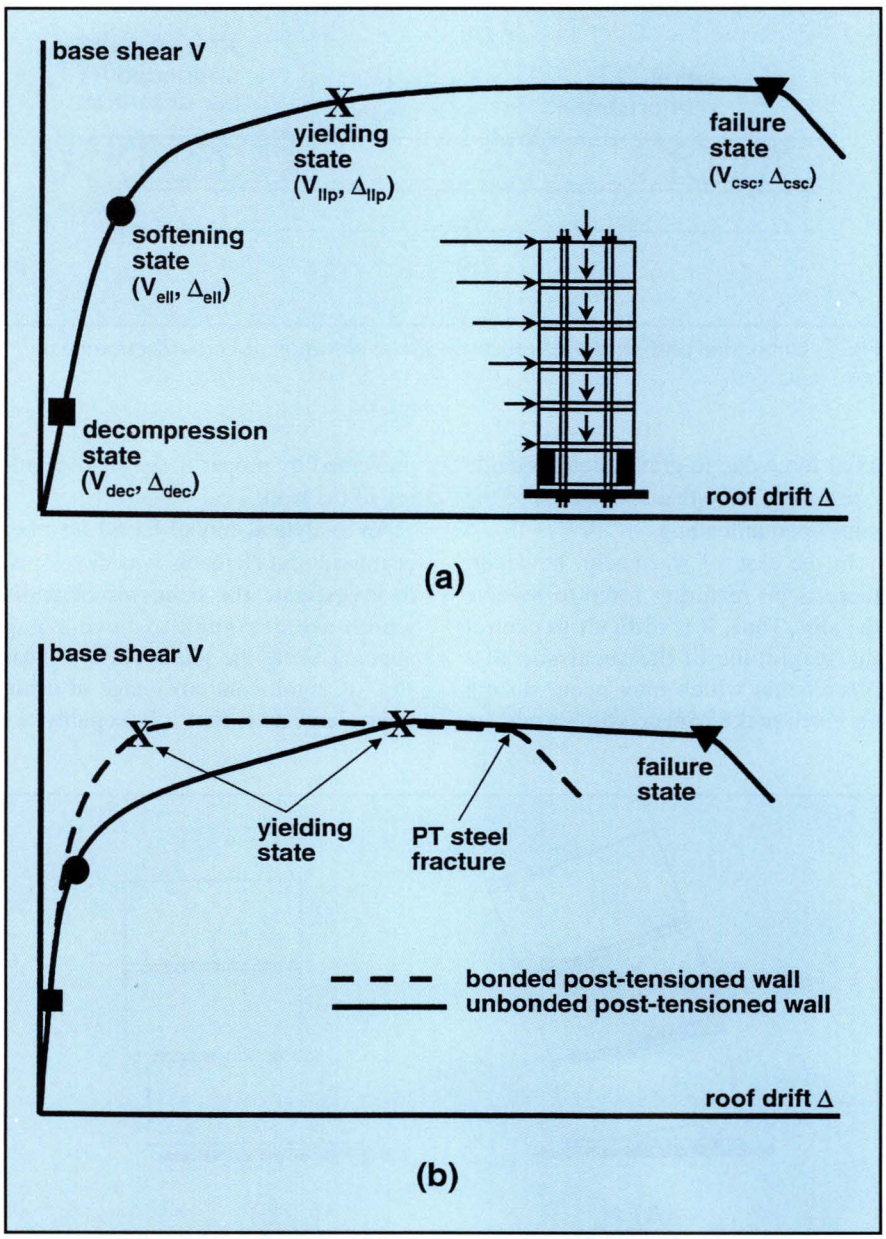

Fig. 3. Base-shear-roof-drift relationship: (a) unbonded post-tensioned precast wall; (b) effect of unbonding of the post-tensioning steel.

Decompression state — This state (indicated by a ■ marker at a base shear and roof drift of V_{dec} and Δ_{dec}, respectively) identifies the initiation of a gap opening along the horizontal joint between the wall and foundation. Gap opening initiates when the initial compression in the concrete due to the post-tensioning force and gravity load is overcome at the extreme edge at the base of the wall.

The decompression state is the beginning of nonlinear behavior of the wall due to gap opening. However, the effect of this nonlinear behavior on the lateral stiffness of the wall is small until the gap opening extends over a significant portion of the length of the horizontal joint.

Softening state — This state (indicated by a ● marker) identifies the beginning of a significant reduction in the lateral stiffness of the wall due to gap opening along the horizontal joints and nonlinear behavior of the concrete in compression. As shown in Fig. 3(a), the reduction in the lateral stiffness of the wall occurs in a smooth and continuous manner. Therefore, an effective linear limit (denoted by V_{ell} and Δ_{ell}) is used to identify the softening state.[5]

The effective linear limit may be governed by gap opening or by nonlinear behavior of the concrete depending on the stress in the concrete due to the post-tensioning force and the gravity load. If the stress in the concrete is small, the effective linear limit is governed by gap opening. If the stress in the concrete is large, the effective linear limit is governed by nonlinear behavior of the concrete.

Yielding state — This state (indicated by a **X** marker) identifies the point at which the strain in the post-tensioning steel first reaches the limit of proportionality. A properly designed wall does not reach the yielding state (denoted by V_{llp} and Δ_{llp}) until a large nonlinear drift has occurred. The nonlinearity results primarily from gap opening along the horizontal joints and nonlinear behavior of the concrete in compression. Up to the yielding state, noticeable damage to the concrete other than spalling of the cover concrete over a small region near the base of the wall is small because the spiral reinforcement provides heavy confinement.

Failure state — This state (indicated by a ▼ marker) identifies axial-flexural failure of the wall which occurs as a result of crushing of the spiral confined concrete (at V_{csc} and Δ_{csc}). Crushing of the spiral confined concrete occurs when the spiral reinforcement fractures. Sufficient spiral reinforcement is provided in the wall panels such that the failure state is reached at a drift significantly larger than the drift at the yielding state.

Effect of Unbonded Post-Tensioning

Fig. 3(b) compares the base-shear-roof-drift behavior of an unbonded post-tensioned wall and a bonded post-tensioned wall. Unbonded post-tensioned construction has the following advantages: (1) yielding of the post-tensioning steel is delayed because the strain in the post-tensioning steel is uniform over the unbonded length; (2) the post-tensioning steel does not transfer significant tensile stresses into the concrete, thus, damage in the wall panels due to cracking is reduced; (3) gap opening along the horizontal joints, primarily at the base of the wall, results in a decrease in the lateral stiffness of the wall (i.e., provides nonlinear behavior) and, thus, period elongation, with little damage to the wall; and (4) fracture of the post-tensioning steel is less likely, and thus, less critical. The effect of unbonded post-tensioning on the behavior of the wall under cyclic lateral load is described below.

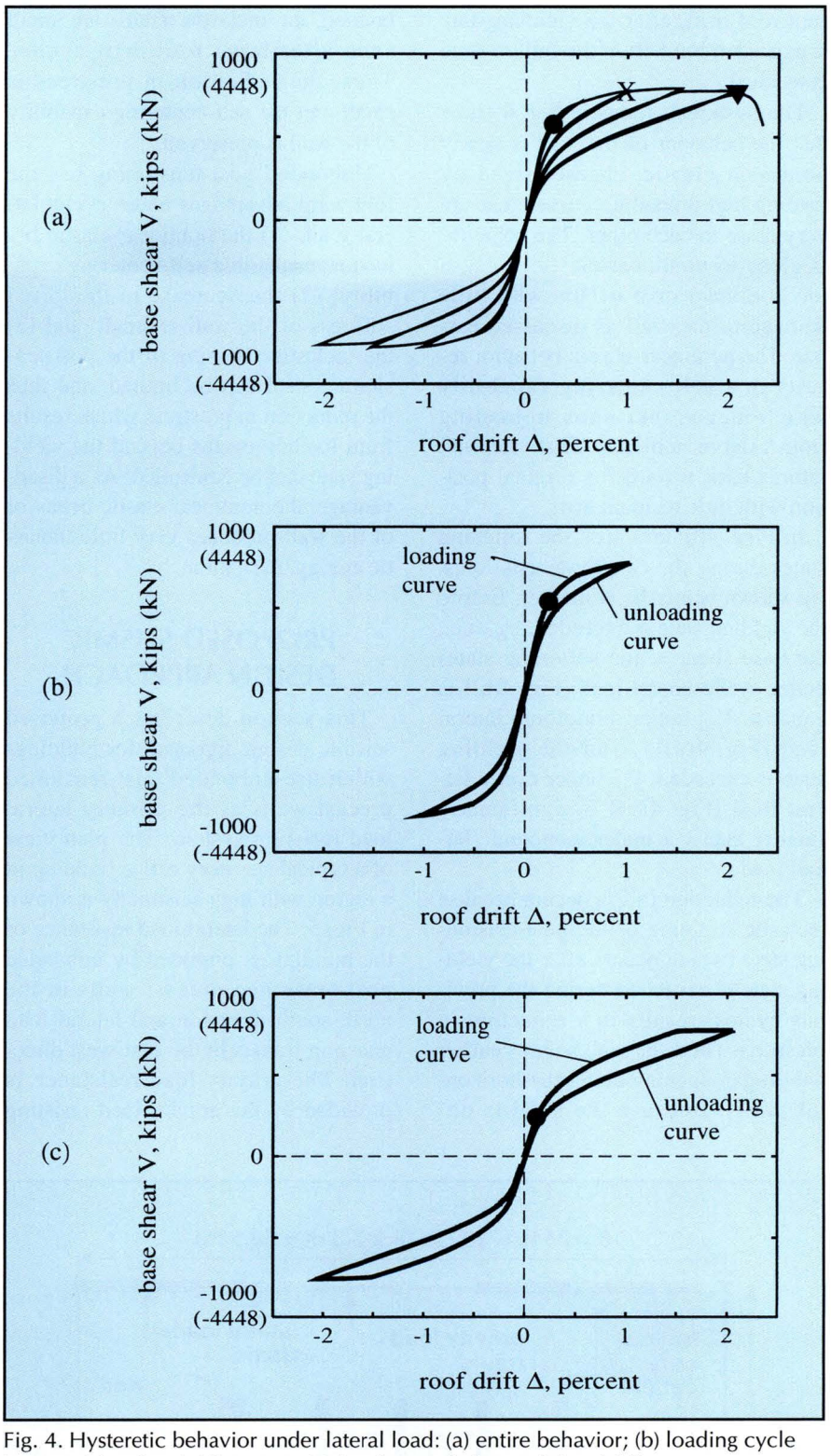

Fig. 4. Hysteretic behavior under lateral load: (a) entire behavior; (b) loading cycle just reaching the yielding state; (c) loading cycle beyond the yielding state.

Behavior Under Cyclic Lateral Load

Fig. 4 shows the base-shear-roof-drift behavior of the wall shown in Fig. 3(a) under cyclic lateral load combined with constant gravity load. The softening, yielding, and failure states under monotonic lateral load are indicated in Fig. 4(a) using the ●, **X**, and ▼ markers, respectively. Fig. 4(b) shows the behavior of the wall during a loading cycle to approximately 1 percent roof drift, just reaching the yielding state. Fig. 4(c) shows the behavior of the wall during a subsequent loading cycle to approximately 2 per-

cent roof drift, after the yielding state is exceeded but before the failure state is reached.

The hysteresis loops in Fig. 4 show that the behavior of the wall is nearly nonlinear-elastic, characterized by loading and unloading curves that are very close to each other. The behavior is close to nonlinear-elastic because the nonlinear drift occurs with little damage to the wall as discussed earlier. The nonlinear-elastic behavior results in a self-centering capability which means that upon unloading from a large nonlinear drift, the wall returns back towards its original position with little residual drift.

In Figs. 4(b) and 4(c), the softening states during the two hysteresis loops are shown using the ● marker. Before the yielding state is exceeded, V_{ell} (i.e., the base shear at the softening state) under cyclic lateral load [Fig. 4(b)] is equal to V_{ell} under monotonic lateral load [Fig. 4(a)]. After the yielding state is exceeded, V_{ell} under cyclic lateral load [Fig. 4(c)] is significantly smaller than V_{ell} under monotonic lateral load.

The reduction in V_{ell} occurs because inelastic straining of the post-tensioning steel (which occurs after the yielding state is exceeded during the previous cycles) results in a reduction in prestress. Thus, the wall softens earlier due to gap opening along the horizontal joints. Because the steel is unbonded, the inelastic strains are small even after large roof drift cycles. Thus, the reduction in prestress is small and the self-centering capability of the wall is preserved.

Unbonded post-tensioning has the following advantages under cyclic lateral load: (1) the nonlinear-elastic behavior results in a self-centering capability; (2) the decrease in the initial stiffness of the wall is small; and (3) the inelastic straining of the post-tensioning steel can be limited, and thus the reduction in prestress which results from loading cycles beyond the yielding state can be controlled. As a disadvantage, the nonlinear elastic behavior of the wall produces very little inelastic energy dissipation.

PROPOSED SEISMIC DESIGN APPROACH

This section describes a proposed seismic design approach for buildings which use unbonded post-tensioned precast walls as the primary lateral load resisting system. The plan view of a typical six-story office building in a region with high seismicity is shown in Fig. 5. The lateral load resistance of the building is provided by unbonded post-tensioned precast walls in the north-south direction and lateral load resisting frames in the east-west direction. The gravity load resistance is provided by the gravity load resisting frames, the walls, and the lateral load resisting frames. The focus in this paper is on the seismic behavior and design of the walls. Seismic behavior and design of unbonded post-tensioned precast frames is discussed by El-Sheikh et al.[8]

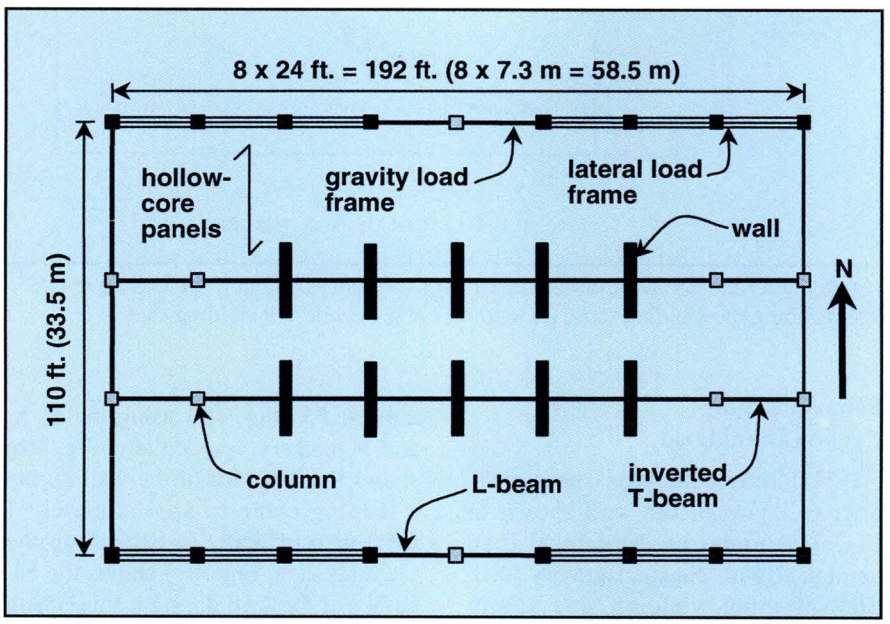

Fig. 5. Typical prototype structure.

The proposed seismic design approach is a performance-based design approach which allows the designer to specify and predict, with reasonable accuracy, the performance (degree of damage) of a building for a specified level of ground motion intensity. This requires the identification of: (1) *seismic performance levels* to describe the expected level of damage in the building during a ground motion; (2) *building limit states and capacities* to describe and quantify the damage in various structural and non-structural elements of the building; (3) *seismic input levels* to describe selected levels of ground motion intensity for a given site; and (4) *structure demands* to quantify roof drift, story drift (i.e., lateral displacement between adjacent floors divided by story height), and base shear demands for the structure.

The design approach uses three seismic performance levels: (1) the "immediate occupancy" performance level, which describes a post-earthquake damage state in which only limited structural and non-structural damage has occurred; (2) the "life safety" performance level, which describes a post-earthquake damage state in which significant damage to the building may have occurred but some margin against either total or partial structural collapse remains; and (3) the "collapse prevention" performance level, which describes a post-earthquake damage state in which the building is on the verge of partial or total collapse.

The building limit states and capacities include limit states and capacities for the unbonded post-tensioned precast walls, the lateral load resisting frames, the gravity load resisting system, and the non-structural elements. The limit states for the walls are: (1) decompression at the base; (2) decrease in the lateral stiffness; (3) spalling of cover concrete near the base; (4) yielding of the post-tensioning steel; (5) attainment of the base moment capacity; (6) reduction in the

prestress due to inelastic straining of the post-tensioning steel; (7) crushing of the concrete confined by spirals; (8) reduction in the lateral load resistance; (9) reduction in the gravity load resistance; (10) shear slip along the horizontal joints; and (11) crushing of the concrete outside the spiral confined region, but inside the region reinforced with wire mesh. Limit States 1, 2, 4, and 7 correspond to the decompression, softening, yielding, and failure states which were described earlier.

The wall design capacities which correspond to these limit states are determined from nonlinear static pushover analyses under combined lateral and gravity loads. The distribution of the lateral loads over the height of the walls is determined from the equivalent lateral force procedure in NEHRP.[9] The gravity loads (i.e., dead and live loads) are determined from the load combinations in NEHRP.

The design approach considers two seismic input levels for a given site: (1) a design level ground motion; and (2) a survival level ground motion (i.e., a maximum intensity ground motion). The design level and survival level ground motions are defined later. The structure demands are specified in terms of demands for the walls corresponding to these levels of ground motion. For the design level ground motion, the wall demands are: (1) the design base shear demand, V_{des}, (used in design to control the axial-flexural behavior); (2) the maximum roof drift demand, Δ_{des}; and (3) the maximum story drift demand, δ_{des}. For the survival level ground motion, the wall demands are: (1) the maximum roof drift demand, Δ_{sur}; and (2) the maximum base shear demand, V_{max} (used in design to prevent shear slip behavior).

Design Objectives

Design objectives relate the seismic performance levels to the seismic input levels described above as shown in Fig. 6(a). The proposed design approach has two objectives: (1) to achieve the immediate occupancy performance level under the design level ground motion; and (2) to achieve the collapse prevention performance level under the survival level ground motion.

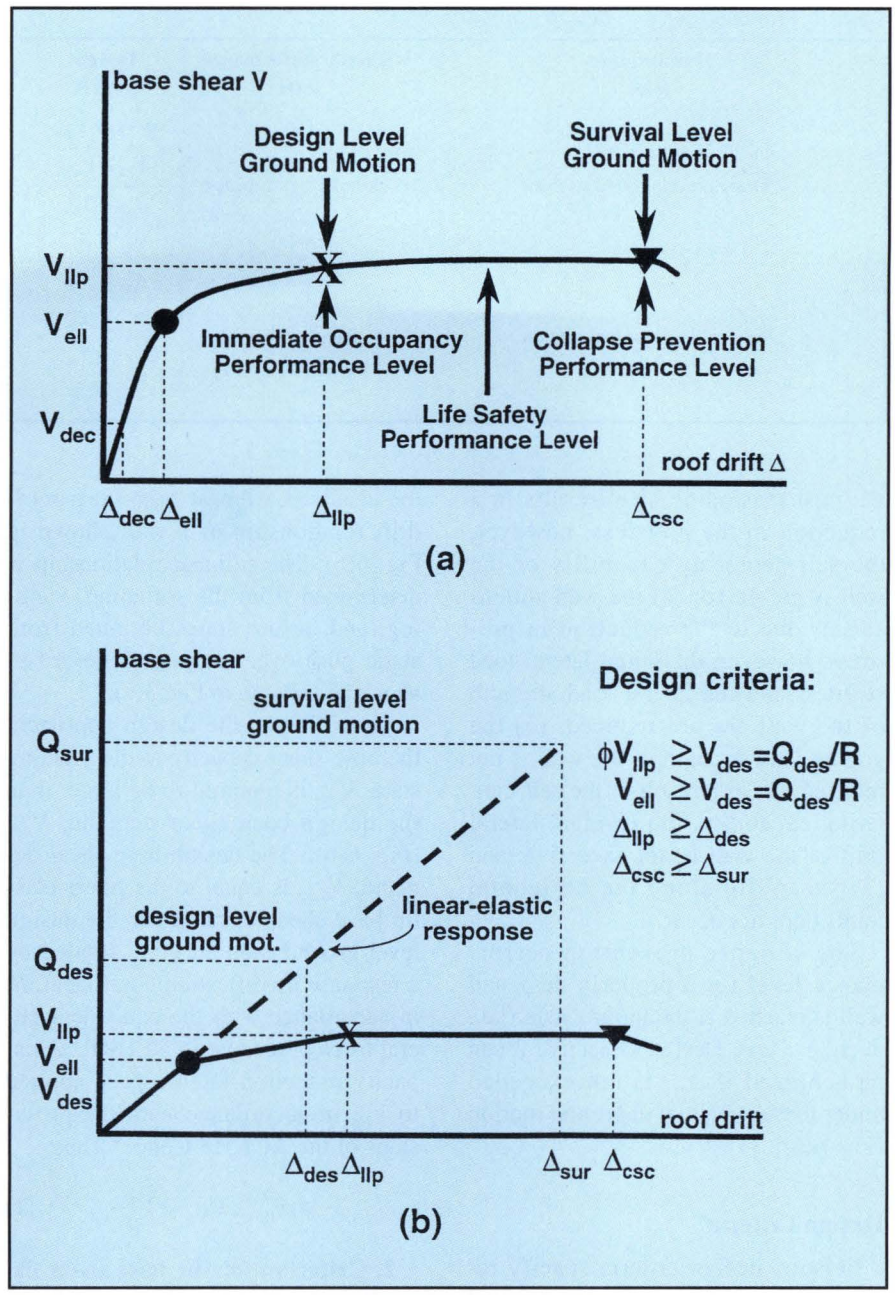

Fig. 6. Proposed seismic design approach: (a) design objectives; (b) design criteria.

The immediate occupancy performance level for the walls is as follows: (1) the wall behavior is nearly elastic, but nonlinear, with the nonlinear behavior being largely due to gap opening along the joints with a small contribution from nonlinear behavior of the concrete in compression; (2) the post-tensioning steel remains linear-elastic; (3) the wall panels remain nearly linear-elastic with little or no cracking, and with nonlinear behavior of concrete in compression occurring only near the bottom corners of the base panel; (4) the initial lateral load stiffness and the lateral load strength of the wall are not reduced; (5) the gravity load strength of the wall is not reduced; and (6) shear slip along the horizontal joints does not occur.

The immediate occupancy performance level for a properly designed wall is reached at the yielding state (i.e., at Δ_{llp}). Thus, Design Objective 1 can be achieved if Δ_{llp} is not exceeded under the design level ground motion [Fig. 6(a)].

The collapse prevention performance level for the walls is as follows: (1) axial-flexural compression failure of the wall does not occur; (2) the post-tensioning steel yields, however, due to unbonding, the inelastic strains are not large; (3) inelastic straining of

Table 1. Proposed seismic design approach.

Seismic input level	Seismic performance level	Design criteria
Design level ground motion	Immediate occupancy	$\phi_f V_{llp} \geq V_{des}$
		$V_{ell} \geq V_{des}$
		$\Delta_{llp} \geq \Delta_{des}$
		$\delta_{des} \leq \delta_{all}$
Survival level ground motion	Collapse prevention	$\Delta_{csc} \geq \Delta_{sur}$
		$\Delta_{ctc} \geq \Delta_{csc}$
		$\phi_s V_{ss} \geq V_{max}$
		$\Delta_{sur} \leq \Delta_g$

the post-tensioning steel results in a reduction in the prestress, however, the self-centering capability of the wall is preserved; (4) the wall softens earlier due to the reduction in prestress, however, the initial lateral load stiffness and the lateral load strength of the wall are not reduced; (5) the gravity load strength of the wall is not reduced; (6) as a result of the self-centering capability, the residual lateral drift of the wall is not excessive; and (7) shear slip along the horizontal joints does not occur.

The collapse prevention performance level for a properly designed wall is reached at the failure state (i.e., at Δ_{csc}). Thus, Design Objective 2 can be achieved if Δ_{csc} is not exceeded under the survival level ground motion [Fig. 6(a)].

Design Criteria

Seismic design criteria specify required comparisons between estimated structure design demands and structure design capacities. If the capacities exceed the demands, the design objectives are achieved. Design of an unbonded post-tensioned precast wall involves establishing wall design demands and providing wall design capacities so that all of the design criteria are satisfied. The design approach includes eight design criteria which are described below and summarized in Table 1. Procedures for estimating the design demands and capacities are not described below in full detail, however, they are given by Kurama et al.[6]

1. Criterion for the base shear capacity at the yielding state, V_{llp} — This design criterion is described using the idealized, trilinear base-shear-roof-drift relationship of a wall shown in Fig. 6(b). The trilinear relationship is determined from the softening, yielding, and failure states obtained from static push-over analysis as described above and shown in Fig. 3(a).

According to the design approach, the base shear capacity at the yielding state, V_{llp}, is required to be larger than the design base shear demand, V_{des} [Fig. 6(b)]. The design base shear demand, V_{des}, is equal to the linear-elastic base shear demand for the design level ground motion, Q_{des}, divided by a response modification coefficient, R, in accordance with the equivalent lateral force procedure in NEHRP.[9] A capacity reduction factor, ϕ_f, is applied to V_{llp} in accordance with the provisions of the ACI 318 Code.[10] Thus:

$$\phi_f V_{llp} \geq V_{des} = \frac{Q_{des}}{R} \qquad (1)$$

2. Criterion for the base shear capacity at the softening state, V_{ell} — The purpose of this criterion is to prevent a premature reduction in the lateral stiffness of the wall. The design approach requires that the base shear capacity at the softening state, V_{ell}, is larger than the design base shear demand, V_{des} [Fig. 6(b)]. A capacity reduction factor is not applied to V_{ell} because the consequences of V_{des} exceeding V_{ell} are not considered to be serious. Thus:

$$V_{ell} \geq V_{des} = \frac{Q_{des}}{R} \qquad (2)$$

3. Criterion for the roof drift capacity at the yielding state, Δ_{llp} — In order to achieve Design Objective 1, the roof drift capacity at the yielding state, Δ_{llp}, is required to be larger than the expected maximum roof drift demand under the design level ground motion, Δ_{des} (Δ_{des} can be estimated from linear-elastic analysis results using an equal displacement assumption as described later). Thus:

$$\Delta_{llp} \geq \Delta_{des} \qquad (3)$$

4. Criterion for the maximum story drift under the design level ground motion, δ_{des} — The purpose of this criterion is to control the initial stiffness of the wall and to control damage to basic access and life safety systems. The NEHRP provisions[9] specify an allowable story drift, δ_{all}. Accordingly, the expected maximum story drift demand under the design level ground motion, δ_{des}, is required to be smaller than δ_{all} (δ_{des} can be estimated from linear-elastic analysis results as described later). Thus:

$$\delta_{des} \leq \delta_{all} \qquad (4)$$

5. Criterion for the roof drift capacity at the failure state, Δ_{csc} — To achieve Design Objective 2, the roof drift capacity at the failure state, Δ_{csc}, is required to be larger than the expected maximum roof drift demand under the survival level ground motion, Δ_{sur} (Δ_{sur} can be estimated from linear-elastic analysis results as described later). Thus:

$$\Delta_{csc} \geq \Delta_{sur} \qquad (5)$$

6. Criterion for the size of the spiral confined region near the base — The purpose of this criterion is to prevent crushing of the concrete in the region reinforced only with wire mesh (Fig. 1). The length and height of the spiral confined wall region near the base should be large enough to prevent crushing of the concrete inside the wire mesh. The design approach requires that the roof drift capacity corresponding to the crushing of the concrete inside the wire mesh, Δ_{ctc}, is larger than the roof drift capacity at the failure state, Δ_{csc}. Thus:

$$\Delta_{ctc} \geq \Delta_{csc} \qquad (6)$$

7. Criterion for the shear slip capacity, V_{ss} — The purpose of this criterion is to prevent shear slip along the horizontal joints. The most critical joint for shear slip is the base-panel-to-foundation joint because the shear demand is maximum at the base while the shear slip capacity is nearly uni-

form over the wall height due to the post-tensioning.[6] The design approach requires that the expected minimum shear slip capacity at the base, V_{ss}, is larger than the expected maximum base shear demand under the survival level ground motion, V_{max} (the estimation of V_{ss} and V_{max} is described later). A capacity reduction factor, ϕ_s, is applied to V_{ss} in accordance with the ACI 318 Code.[10] Thus:

$$\phi_s V_{ss} \geq V_{max} \quad (7)$$

8. Criterion for the maximum roof drift under the survival level ground motion, Δ_{sur} — The purpose of this criterion is to prevent premature failure of the gravity load resisting system which is not part of a lateral load resisting system, due to excessive drift. Design of the gravity load system is not addressed in this paper. However, it is assumed that the gravity load system can be designed to sustain a roof drift of $\Delta_g = 2.5$ percent. The design approach requires that the expected maximum roof drift demand under the survival level ground motion, Δ_{sur} is smaller than Δ_g. Thus:

$$\Delta_{sur} \leq \Delta_g = 2.5 \text{ percent} \quad (8)$$

PROPOSED SEISMIC DESIGN PROCEDURE

This section describes the proposed seismic design procedure for unbonded post-tensioned precast walls. This procedure is based on a parametric investigation which was conducted to determine how the wall design capacities V_{llp}, V_{ell}, Δ_{llp}, and Δ_{csc} are affected by changes in wall design properties. The wall design properties that were considered include: (1) initial stress in the post-tensioning steel, f_{pi}; (2) total area of the post-tensioning steel, A_p; (3) wall length, l_w; (4) location of the post-tensioning steel; (5) unbonded length of the post-tensioning steel, l_{unb}; (6) wall panel spiral reinforcement ratio, ρ_{sp}; (7) amount of gravity load, G; (8) unconfined concrete compressive strength, f_c'; and (9) wall thickness, t_w.

Approximately 200 nonlinear static push-over analyses of a number of walls which differ in only one or two of the design properties were conducted. The properties of the walls which were used in this parametric investigation are described in detail by Kurama et al.[5] The design capacities of the walls were determined from the base-shear-roof-drift relationships obtained from the analyses. Figs. 7(a) through 7(g) show the base-shear-roof-drift relationships of some of the walls. The base shear resistance of the walls is normalized by V_{llp} of a selected wall[5] with a particular set of properties, for which V_{llp} = 358 kips (1592 kN) [see Fig. 7(e)].

The results in Fig. 7 suggest relationships between the wall design properties and the wall design capacities. For example, Figs. 7(a) and 7(b) show that V_{ell} is significantly affected by f_{pi} and A_p.

Fig. 7(c) shows the normalized base-shear-roof-drift relationship of four walls where both f_{pi} and A_p are varied such that the total post-tensioning force, P_i, remains constant ($P_i = A_p f_{pi}$). This figure shows that V_{ell} remains constant when P_i remains constant. Thus, after selecting trial wall dimensions (i.e., wall length, l_w and wall thickness, t_w), the first step toward a design that satisfies the design criteria is to set f_{pi} to a desired value (usually 55 to 65 percent of the ultimate strength of the post-tensioning steel, f_{pu}). Then, A_p is determined such that $V_{ell} \leq V_{des}$ to satisfy Design Criterion 2.

Figs. 7(b) and 7(d) show that V_{llp} is significantly affected by A_p and l_w. Thus, the next step in design is to check that A_p and l_w are large enough so that $\phi_f V_{llp} \geq V_{des}$ to satisfy Design Criterion 1.

The next step in design is to check that $\delta_{des} \leq 1.5$ percent and $\Delta_{sur} \leq 2.5$ percent to satisfy Design Criteria 4 and 8, respectively. Deflections δ_{des} and Δ_{sur} are estimated from the linear-elastic lateral stiffness of the wall estimated using the wall length, l_w, and the wall thickness, t_w.

Figs. 7(a), 7(e), and 7(f) show that Δ_{llp} is significantly affected by f_{pi}, l_{unb}, and the location of the post-tensioning steel. Typically, l_{unb} is equal to the wall height to take full advantage of unbonded construction. Thus, the next step in design is to check that f_{pi} and the location of the post-tensioning steel are such that $\Delta_{llp} \geq \Delta_{des}$ to satisfy Design Criterion 3. It is recommended that the post-tensioning steel is located between the two regions of spiral confined concrete so that the spiral confined regions are not weakened by the presence of the post-tensioning ducts.

The next step in design is to check that $\phi_s V_{ss} \leq V_{max}$ to satisfy Design Criterion 7. This is discussed in more detail later.

Fig. 7(g) shows that Δ_{csc} is significantly affected by the amount of spiral reinforcement, ρ_{sp}. Thus, the final step in design is to provide sufficient spiral reinforcement so that $\Delta_{csc} \geq \Delta_{sur}$ to satisfy Design Criterion 5. Based on the nonlinear static and nonlinear dynamic analyses conducted in this research, it is recommended that interlocking spiral reinforcement is provided over a length equal to, at least, one-quarter of the wall length near each bottom corner and over a height greater than or equal to the first story, so that $\Delta_{ctc} \geq \Delta_{csc}$ to satisfy Design Criterion 6.

DESIGN OF PROTOTYPE WALLS

Six six-story prototype walls were designed using the design approach and the design procedure described above. The prototype walls were designed for sites in two different seismic regions (regions with high seismicity and regions with moderate seismicity) and for sites with three different soil characteristics (stiff soil, medium soil, and soft soil characteristics). The prototype walls were designed using the 1991 edition of the NEHRP provisions[9] as described below. This edition of the NEHRP provisions was used because the prototype walls were designed before the 1994 edition was published in May 1995.

The design level and survival level ground motions which were used in the design of the prototype walls were determined from the 1991 edition of the NEHRP provisions. The design level ground motion is the NEHRP design ground motion and has a 90 percent probability of not being exceeded in 50 years, corresponding approximately to a 500-year return period. The prototype walls were designed for a design level ground motion with a peak acceleration of 0.40g and 0.10g

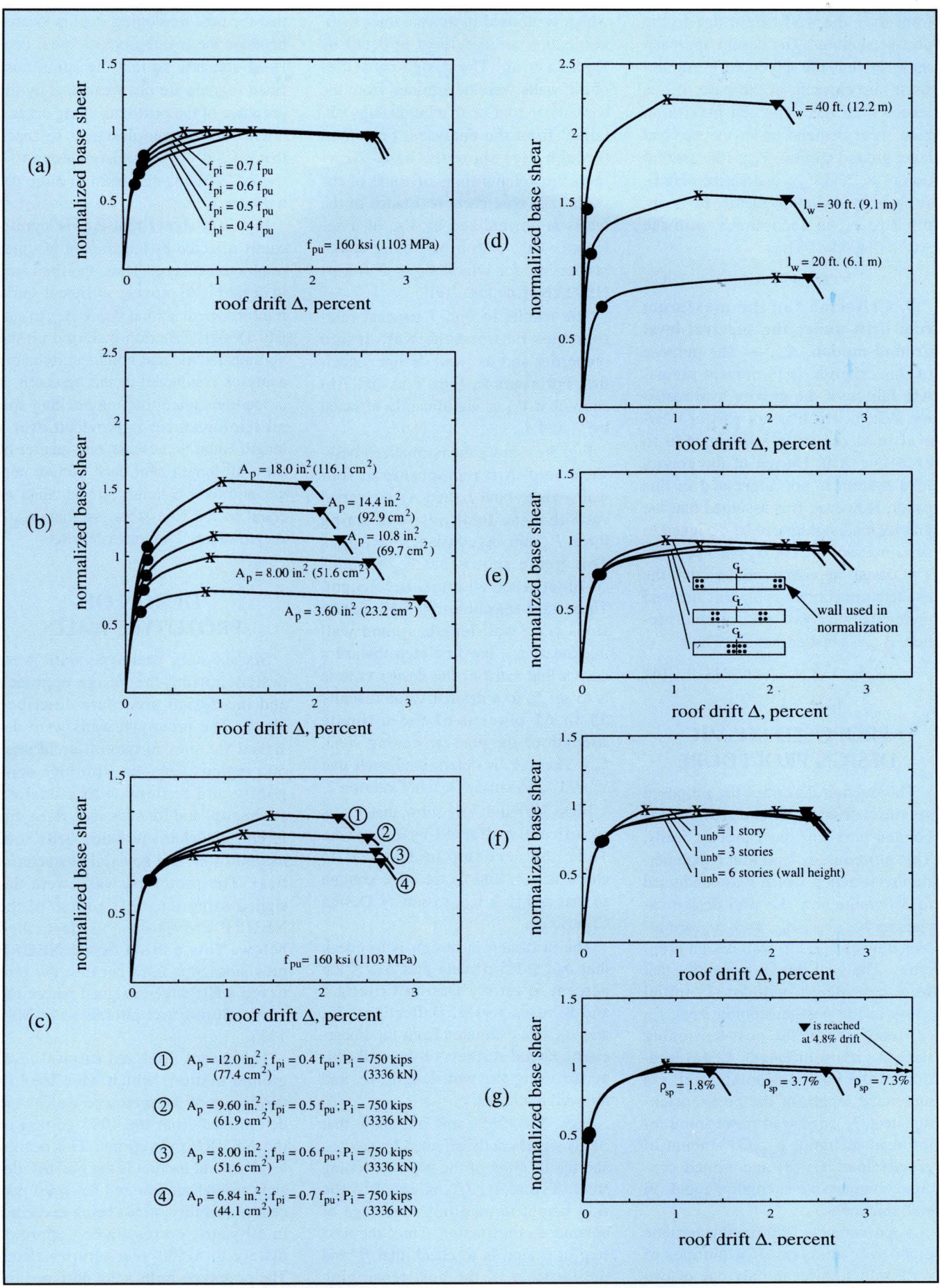

① A_p = 12.0 in.^{2} (77.4 cm^2); $f_{pi} = 0.4\ f_{pu}$; P_i = 750 kips (3336 kN)

② A_p = 9.60 in.^{2} (61.9 cm^2); $f_{pi} = 0.5\ f_{pu}$; P_i = 750 kips (3336 kN)

③ A_p = 8.00 in.^{2} (51.6 cm^2); $f_{pi} = 0.6\ f_{pu}$; P_i = 750 kips (3336 kN)

④ A_p = 6.84 in.^{2} (44.1 cm^2); $f_{pi} = 0.7\ f_{pu}$; P_i = 750 kips (3336 kN)

Fig. 7. Effect of wall structural properties on wall design capacities: (a) initial steel stress, f_{pi}; (b) total steel area, A_p; (c) f_{pi} and A_p; (d) wall length, l_w; (e) steel location; (f) unbonded length, l_{unb}; (g) spiral ratio, ρ_{sp}.

in regions of high seismicity and moderate seismicity, respectively.

The survival level ground motion has approximately a 90 percent probability of not being exceeded in 250 years. The prototype walls were designed for a survival level ground motion with a peak acceleration of $1.0g$ and $0.25g$ in regions of high seismicity and moderate seismicity, respectively. Quantification of these ground motions is described by Kurama et al.[6]

In the design of the prototype walls, $R = 4.5$ was used in Design Criteria 1 and 2, and $\delta_{all} = 1.5$ percent was used in Design Criterion 4 as specified by the 1991 edition of the NEHRP provisions.[9] Capacity reduction factors of $\phi_f = 0.75$ (for axial compression and flexure) and $\phi_s = 0.85$ (for shear) were used in Design Criteria 1 and 7, respectively, in accordance with the ACI 318 Code.[10]

Additional work is needed to investigate the effects of the differences between the 1991 edition of the NEHRP provisions and the current 1997 edition on the seismic design and dynamic response evaluation of the prototype walls. There are differences in the design level ground motion, in the coefficients related to the site soil characteristics, and in the R and δ_{all} values specified by the two editions.

In the 1991 edition, $R = 4.5$ is specified for reinforced concrete bearing wall systems and $\delta_{all} = 1.5$ percent is specified for buildings with more than

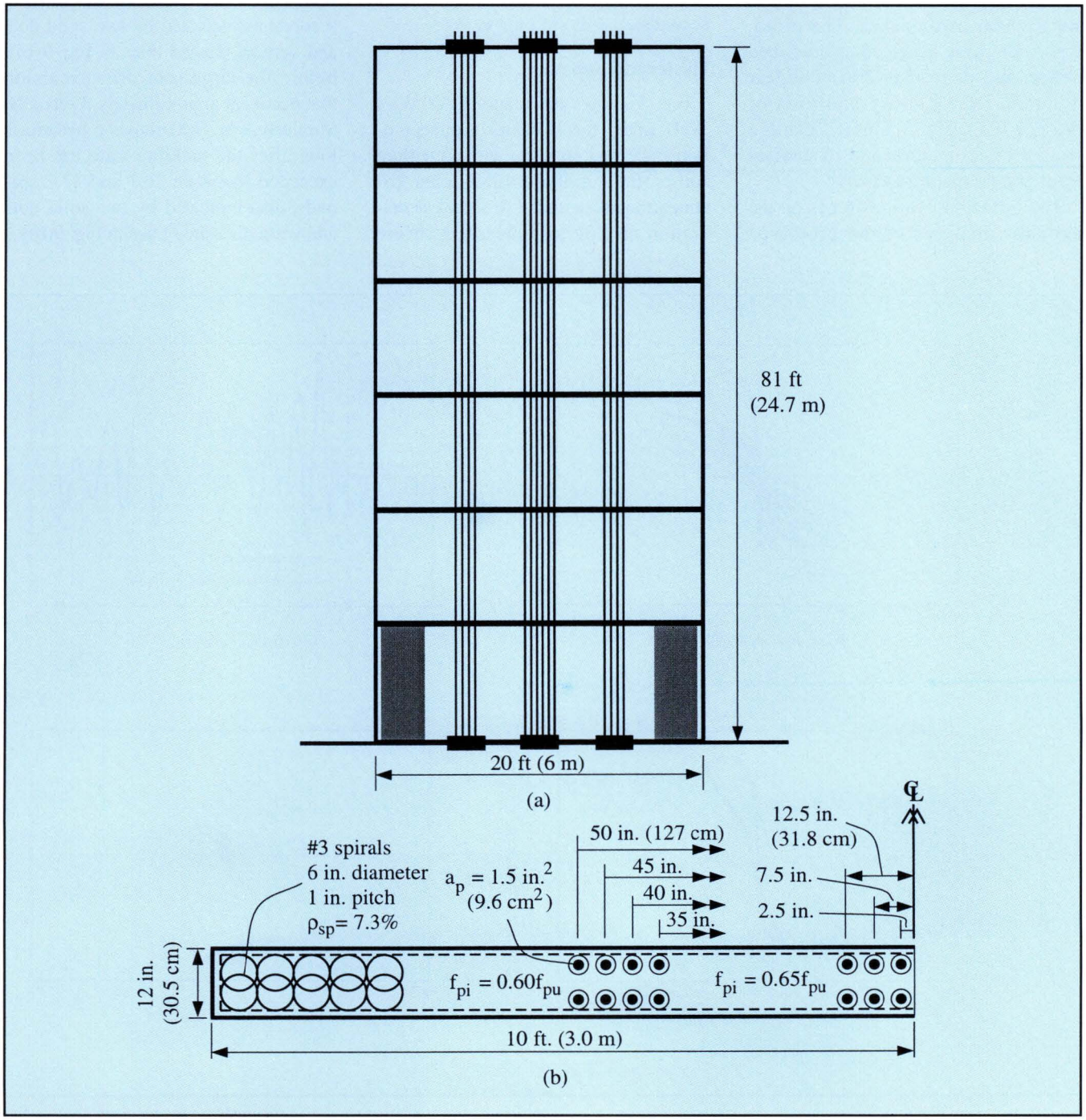

Fig. 8. Properties of Wall WH1: (a) elevation; (b) cross section near base (enlarged).

four stories. In the 1997 edition, R = 5.5 is specified for special reinforced concrete bearing walls and δ_{all} = 2.0 percent is specified for buildings with more than four stories. There are additional differences in the combination of earthquake loads and gravity loads in the two editions.

BEHAVIOR OF PROTOTYPE WALLS UNDER EARTHQUAKE LOAD

This section describes the expected dynamic response of the prototype walls under earthquakes. The prototype walls were designed as described above, and more than 200 nonlinear dynamic time-history analyses of these walls were conducted using a total of 15 design level and 15 survival level ground motion records.[6]

The following sections focus on the dynamic analyses of the prototype walls designed for regions with high seismicity. The dynamic analyses of the prototype walls that were designed for regions with moderate seismicity are discussed by Kurama et al.[6] Fig. 8 shows the properties of one of the prototype walls (referred to as Wall WH1) designed for a region with high seismicity and a site with a medium soil profile, for the prototype structure shown in Fig. 5. Most of the discussion in this section is based on this wall. The dynamic analyses were conducted with a viscous damping ratio of 3 percent and a time step of 0.01 seconds.

Hysteretic Behavior

Fig. 9 shows the response of Wall WH1 under the Hollister ground motion (recorded on a site with a medium soil profile during the 1989 Loma Prieta earthquake) scaled to a peak acceleration of 1.0g to represent a severe survival level ground motion. This ground motion was selected from a larger set of ground motions and has the potential to severely damage Wall WH1.[6] The behavior of Wall WH1 under static cyclic lateral load was shown previously in Fig. 4.

Fig. 9(a) shows the base-moment-base-rotation hysteretic response and the heavy solid line in Fig. 9(b) shows the roof-drift time-history. Figs. 9(c) and 9(d) show two hysteresis loops taken from Fig. 9(a). Fig. 9(c) shows a hysteresis loop before the yielding state is reached [between 6.3 and 7.5 seconds as indicated by two solid dots and vertical dashed lines in Fig. 9(b)], before the large roof drift excursion that occurs at approximately 8 seconds. Similarly, Fig. 9(d) shows a hysteresis loop after the yielding state has been exceeded [between 26.1 and 27.7 seconds, also indicated by two solid dots and vertical dashed lines in Fig. 9(b)].

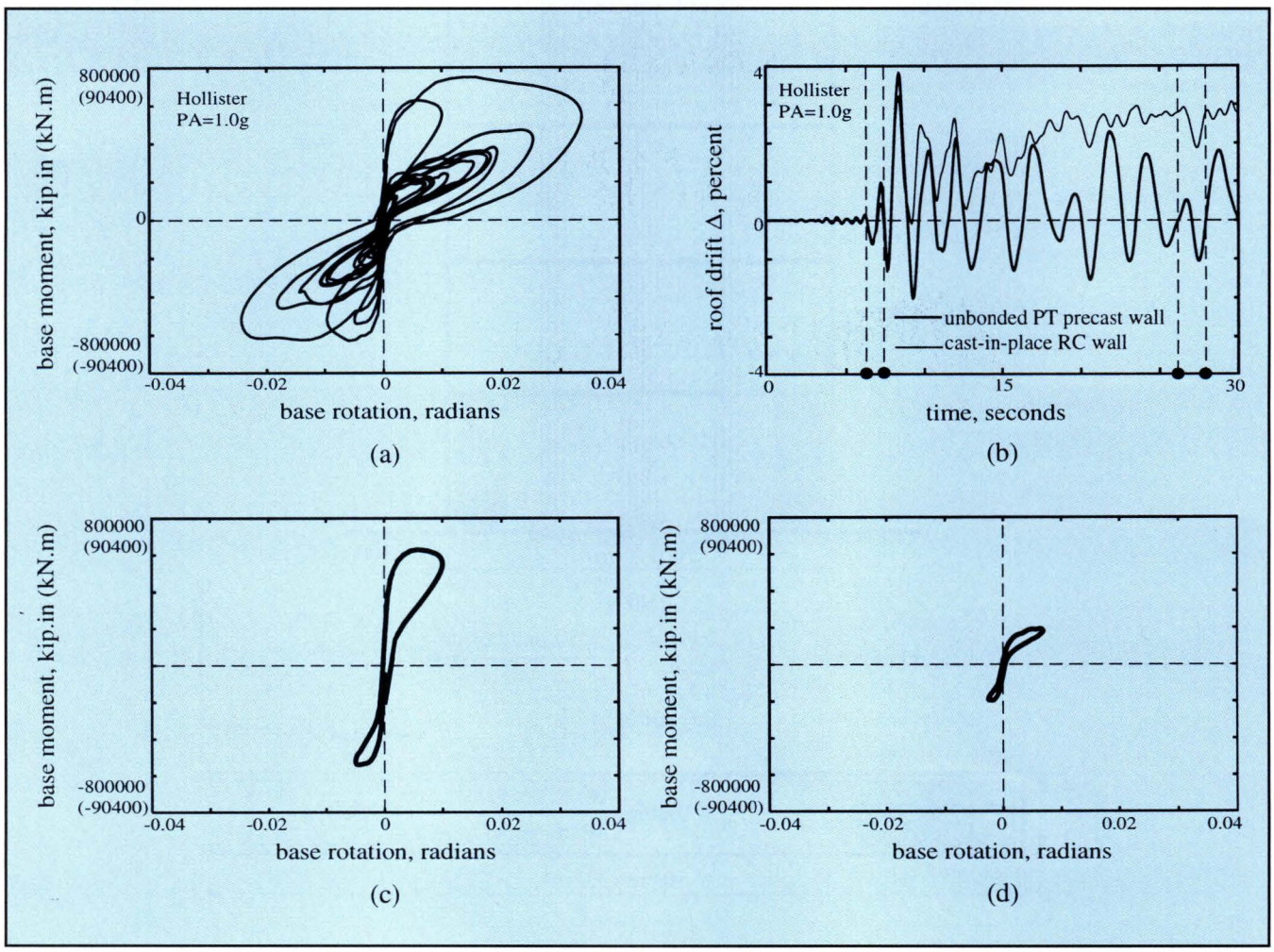

Fig. 9. Behavior under earthquake load: (a) base-moment-base-rotation hysteresis; (b) roof-drift time-history; (c) response between time = 6.3 and 7.5 seconds; (d) response between time = 26.1 and 27.7 seconds.

The shape of the hysteresis loops under dynamic loading (Fig. 9) are similar to those under static cyclic loading (Fig. 4). The hysteresis loop in Fig. 9(c) dissipates more energy than the hysteresis loop in Fig. 4(b) because of the 3 percent viscous damping that was used in the dynamic analysis.

Figs. 9(c) and 9(d) show that softening of the wall occurs at a smaller base moment after the yielding state has been exceeded in a previous cycle (as discussed earlier using Fig. 4). Because of the early softening, the maximum base moment reached during the hysteresis loop in Fig. 9(d) is smaller than the maximum base moment reached during the hysteresis loop in Fig. 9(c) (even though the roof drifts reached during the two loops are similar). It is noted that the reduction in the maximum base moment reached in Fig. 9(d) indicates a reduction in the moment at which the wall softens, and not a reduction in the ultimate strength of the wall. As shown in Fig. 4(c), there is no significant reduction in the ultimate strength of the wall until the failure state is exceeded.

Fig. 9(b) shows a comparison between the roof-drift time-history of Wall WH1 (heavy solid line) and the roof-drift time-history of a cast-in-place reinforced concrete wall (light solid line). The cast-in-place wall has the same strength, initial stiffness, drift capacity, initial fundamental period, and viscous damping as Wall WH1. Thus, the only difference between the walls is their hysteretic behavior under lateral load. The hysteretic behavior of Wall WH1 is shown in Fig. 4. The inelastic energy dissipation of the cast-in-place wall is approximately twice the inelastic energy dissipation of Wall WH1. However, the cast-in-place wall does not have a self-centering capability.[6]

Three important differences are observed between the response of Wall WH1 and the cast-in-place wall: (1) the maximum roof drift of Wall WH1 is larger than that of the cast-in-place wall; (2) the response of Wall WH1 decays (damps out) less rapidly resulting in a large number of large drift cycles; and (3) Wall WH1 oscillates around the zero-drift position, whereas, the cast-in-place wall accumulates a significant residual drift (residual roof drift ≈ 3 percent).

Based on the results of the dynamic analyses (using seven ground motions recorded on sites with a medium soil profile), the maximum roof drift of Wall WH1 is, on average, 38 percent larger than that of the cast-in-place wall under design level ($0.40g$) ground motions, and 41 percent larger than that of the cast-in-place wall under survival level ($1.0g$) ground motions.[6]

Maximum Roof Drift and Story Drift Demands

Satisfactory seismic response of an unbonded post-tensioned precast wall depends on the maximum roof drift reached during a ground motion. For a design level ground motion, if the maximum roof drift exceeds the expected maximum roof drift demand, Δ_{des}, or if the maximum story drift exceeds the expected maximum story drift demand, δ_{des}, unexpected structural and/or nonstructural damage may occur. For a survival level ground motion, if the maximum roof drift exceeds the expected maximum roof drift demand, Δ_{sur}, the wall may suffer an axial-flexural compression failure due to crushing of the spiral confined concrete. Thus, accurate estimates of Δ_{des}, δ_{des}, and Δ_{sur} are needed for design.

In the design of the prototype walls, Δ_{des}, δ_{des}, and Δ_{sur} were estimated using an equal displacement assumption. According to the equal displacement assumption, a nonlinear system and a linear-elastic system with the same initial fundamental (first mode) period have similar maximum drift demands for a given ground motion. Thus, Δ_{des}, δ_{des}, and Δ_{sur} are estimated from linear-elastic analysis results [Fig. 6(b)].

For the linear-elastic analysis, the distribution of the lateral forces over the height of the wall is determined using the equivalent lateral force procedure in NEHRP.[9] The gravity loads (i.e., dead and live loads) are determined from the load combinations in NEHRP. The deflections Δ_{des} and δ_{des} are the roof drift and the maximum story drift (which occurs in the top story) at a base shear equal to the linear-elastic base shear demand for the design level ground motion, Q_{des} [Fig. 6(b)]. Δ_{sur} is the roof drift at a base shear equal to the linear-elastic base shear demand for the survival level ground motion, Q_{sur}. Q_{des} and Q_{sur} are calculated using the NEHRP design response spectrum[9] scaled to represent either the design level or the survival level ground motion.

The equal displacement assumption is usually applicable to structural systems with wide and stable (i.e., ductile) hysteresis loops, with fundamental periods longer than, approximately, 0.5 seconds, and located on sites with a stiff soil profile.[11] The prototype walls have fundamental periods which are longer than 0.5 seconds and have stable but narrow hysteresis loops. The applicability of the equal displacement assumption to the prototype walls is discussed below using Fig. 10.

Figs. 10(a) and (b) show the roof-drift time-history of Wall WH1 under the Newhall ground motion (recorded on a site with a medium soil profile during the 1994 Northridge earthquake) scaled to peak accelerations of $0.40g$ and $1.0g$ to represent design level and survival level ground motions, respectively. Similarly, Figs. 10(c) and (d) show the roof-drift time-history of another prototype wall, Wall WH4, designed for a region with high seismicity and a site with a soft soil profile, under the Foster City ground motion (recorded on a site with a soft soil profile during the 1989 Loma Prieta earthquake) scaled to $0.40g$ and $1.0g$. Similar to the Hollister ground motion, the Newhall and Foster City ground motions were selected from a larger set of ground motions and have the potential to severely damage Walls WH1 and WH4.[6] Walls WH1 and WH4 have fundamental periods of 0.65 and 0.50 seconds, respectively.

Fig. 10 shows that the Δ_{des} and Δ_{sur} values estimated using the equal displacement assumption (indicated by the dashed horizontal lines) underestimate the maximum roof drift reached during the dynamic analyses.

The maximum roof drift demand for Wall WH1 estimated using the equal displacement assumption is Δ_{des} = 0.81 percent and Δ_{sur} = 2.0 percent for

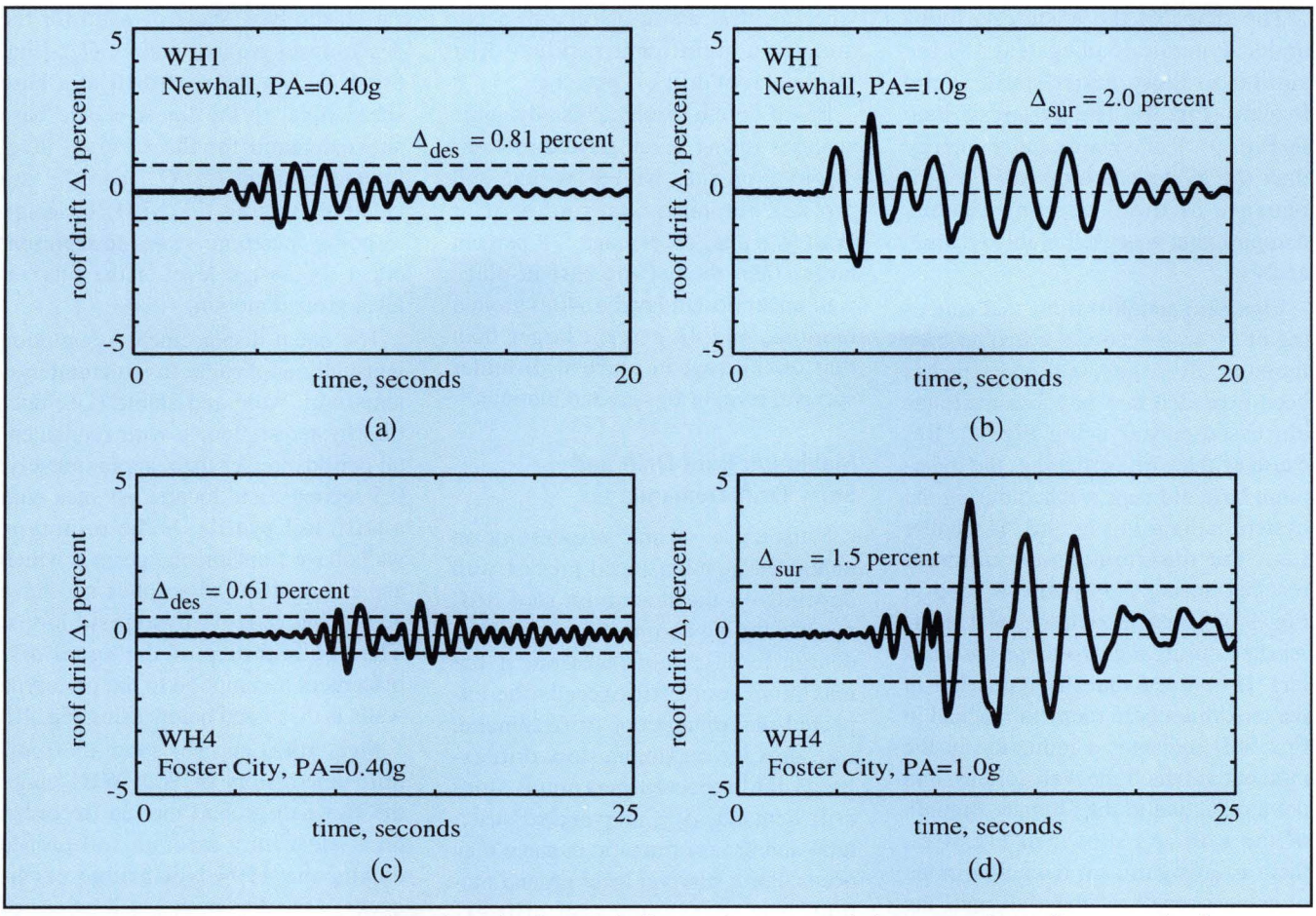

Fig. 10. Roof-drift time-history: (a) Wall WH1 under the Newhall ground motion scaled to 0.40*g*; (b) Wall WH1 under the Newhall ground motion scaled to 1.0*g*; (c) Wall WH4 under the Foster City ground motion scaled to 0.40*g*; (d) Wall WH4 under the Foster City ground motion scaled to 1.0*g*.

the design level and survival level ground motions, respectively. The average maximum roof drift obtained from the dynamic analyses (using seven ground motions recorded on sites with a medium soil profile) is 0.93 percent and 3.2 percent for the design level (0.40*g*) and survival level (1.0*g*) ground motions, respectively.[6]

Similarly for Wall WH4, the maximum roof drift demand estimated using the equal displacement assumption is Δ_{des} = 0.61 percent and Δ_{sur} = 1.5 percent for the design level and survival level ground motions, respectively. The average maximum roof drift obtained from the dynamic analyses (using three ground motions recorded on sites with a soft soil profile) is 0.91 and 3.9 percent for the design level (0.40*g*) and survival level (1.0*g*) ground motions, respectively.[6]

The difference between the estimated maximum roof drift demand and the maximum roof drift from the dynamic analyses is larger for the survival level ground motions than for the design level ground motions, and is larger for walls designed for sites with a soft soil profile than for sites with a medium soil profile. The results also indicate that there is a large scatter in the maximum roof drift demand for sites with medium or soft soil profiles, particularly for the survival level ground motions.

The dynamic analysis results show that the equal displacement assumption would, on average, provide a reasonable estimate of the maximum roof drift demands for walls designed for sites with a stiff soil profile but not for sites with medium or soft soil profiles. Improved methods to estimate the maximum roof drift demands for walls designed for sites with medium or soft soil profiles are needed for design.

Post-Tensioning Steel Forces

This section investigates the reduction in prestress that occurs due to inelastic straining of the post-tensioning steel during loading cycles beyond the yielding state as described earlier. Fig. 11(a) shows the time-history of the total force in the post-tensioning steel in Wall WH1 during the Newhall ground motion scaled to peak accelerations of 0.40*g* and 1.0*g* representing design level and survival level ground motions, respectively. The total post-tensioning steel force is normalized with respect to the total ultimate strength of the post-tensioning steel.

Fig. 11(a) shows that there is a significant reduction in the total post-tensioning steel force under the survival level (1.0*g*) ground motion. This is explained below using Fig. 11(b), which shows the roof-drift time-histories of the wall during the two ground motions [which are also shown in Figs. 10(a) and 10(b)]. The horizontal lines in Fig. 11(b) indicate the roof drift at which the yielding state is reached (i.e., Δ_{llp} = 0.82 percent) during static push-over analysis of the wall.

The local maxima on the post-tensioning steel force time-histories in Fig. 11(a) correspond to local maxima in the roof-drift time-histories in Fig. 11(b) (i.e., maximum total post-tensioning steel forces are reached at maximum roof drift). The local minima on the post-tensioning steel force time-histories correspond to times of zero roof drift. The reduction in the total post-tensioning steel force at zero roof drift which occurs in Fig. 11(a) is a measure of the reduction in prestress due to inelastic straining of the post-tensioning steel.

During the design level ($0.40g$) ground motion, the maximum inelastic strain reached in the post-tensioning steel is very small and, thus, the corresponding reduction in prestress is very small. As shown in Fig. 11(a), there is a very small reduction in prestress at around 6 seconds which occurs as a result of the inelastic straining of the post-tensioning steel when the roof drift at the yielding state (Δ_{llp}) is exceeded as shown in Fig. 11(b).

During the survival level ($1.0g$) ground motion, significant yielding of the post-tensioning steel occurs, resulting in a significant reduction in prestress. The solid line in Fig. 11(b) shows a large positive roof drift cycle around 4 seconds which significantly exceeds Δ_{llp}. This results in inelastic straining of the post-tensioning steel and reduction of the total post-tensioning steel force at zero roof drift as shown in Fig. 11(a), thus, a reduction in prestress occurs. In the two subsequent roof drift cycles, Δ_{llp} is exceeded even further, resulting in additional inelastic straining of the post-tensioning steel, and thus, additional reduction in prestress. The roof drift cycles that follow are smaller and do not cause further reduction in prestress.

As described earlier, the proposed design approach requires that Δ_{llp} is not reached under the design level ground motion [Fig. 6(a)]. Thus, reduction in prestress under the design level ground motion should not occur. Under the survival level ground motion, roof drift cycles that significantly exceed Δ_{llp} are allowed by the design approach, possibly resulting in significant reduction in prestress as shown in Fig. 11(a).

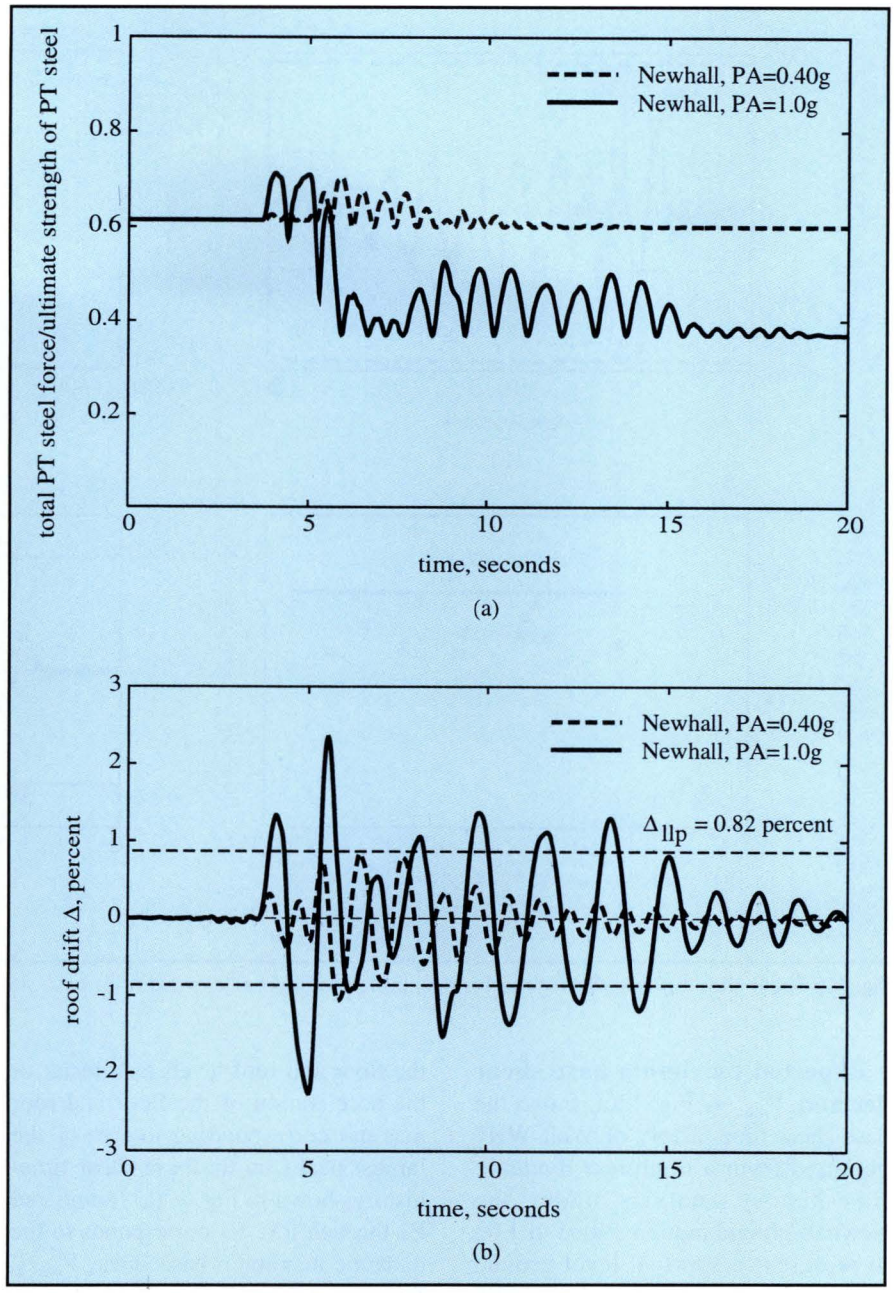

Fig. 11. Post-tensioning steel forces: (a) time-history of normalized total post-tensioning (PT) steel force; (b) time-history of roof drift.

The reduction in prestress has two important effects on the dynamic response: (1) it changes the hysteretic behavior of the wall as shown in Fig. 9(a) and described using Fig. 4 (i.e., earlier softening of the wall occurs, however, the self-centering capability is preserved); and (2) it significantly reduces the shear slip capacity of the wall as discussed in the next section. It is important that the reduction in prestress is considered in the seismic design of walls for the survival level ground motion. The proposed design approach includes a method to estimate the maximum reduction in prestress under the survival level ground motion, which can be found in Kurama et al.[6]

Shear Slip

As described earlier, the proposed design approach requires that shear slip along the horizontal joints is prevented (i.e., $\phi_s V_{ss} \geq V_{max}$). This requires an estimate of the expected maximum base shear demand under the survival level ground motion, V_{max} and the expected minimum shear slip capacity of the base-panel-to-foundation joint, V_{ss}. This is described below.

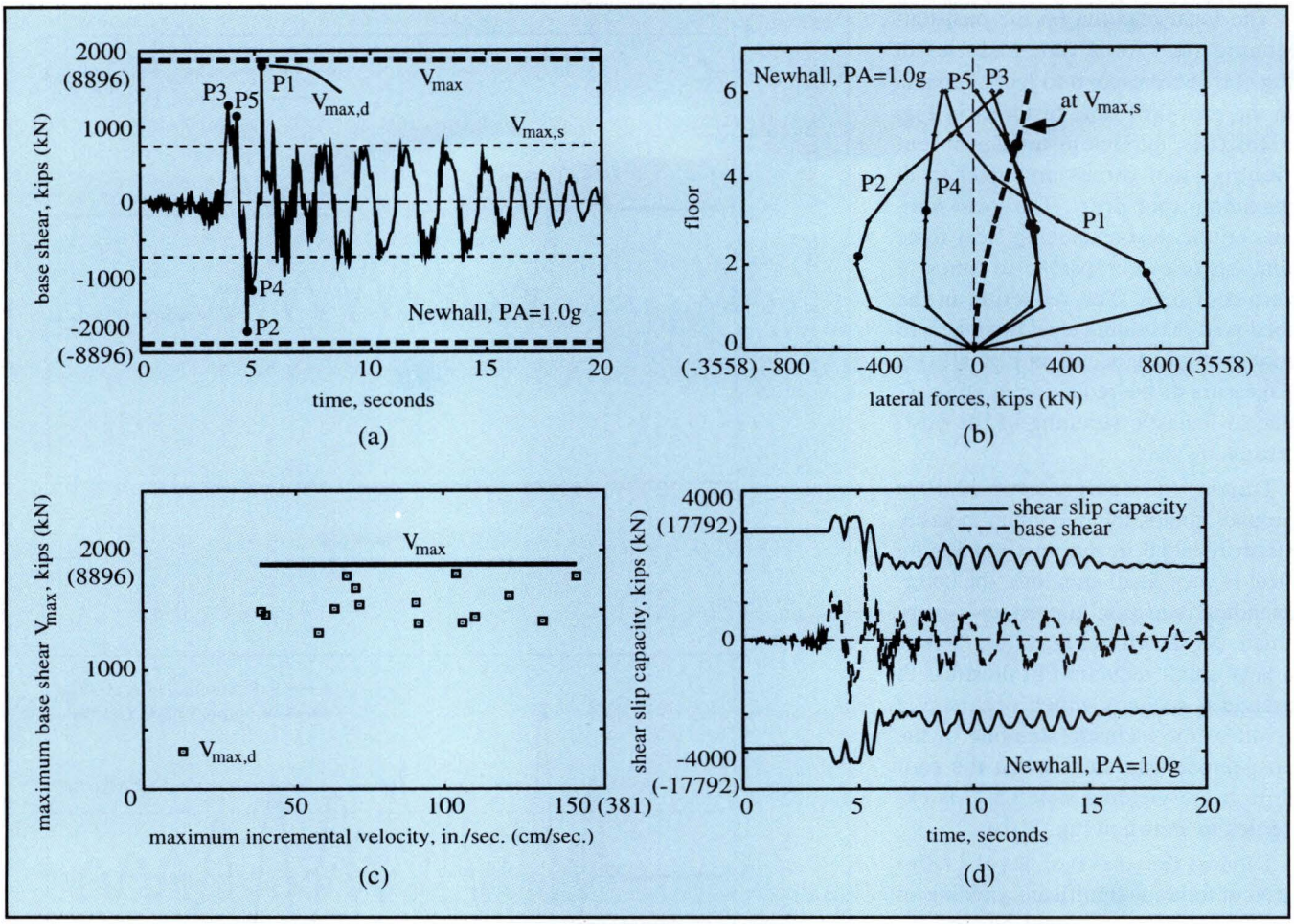

Fig. 12. Shear slip: (a) base-shear time-history; (b) lateral forces; (c) maximum base shear; (d) shear slip capacity.

Expected maximum base shear demand, V_{max} — Fig. 12(a) shows the base shear time-history of Wall WH1 obtained from a nonlinear dynamic time-history analysis under the Newhall ground motion scaled to 1.0*g* to represent a survival level ground motion. The light dashed horizontal lines indicate the maximum base shear reached during a nonlinear static push-over analysis of the wall under combined gravity loads and lateral loads.

In the nonlinear static push-over analysis, the distribution of the lateral loads over the height of the wall is based on the equivalent lateral force procedure in NEHRP.[9] The maximum base shear reached during the static analysis is referred to as the static maximum base shear, $V_{max,s}$, and the maximum base shear reached during the dynamic analysis is referred to as the dynamic maximum base shear, $V_{max,d}$. Fig. 12(a) shows that $V_{max,d}$ is significantly larger than $V_{max,s}$.

Fig. 12(b) shows the lateral inertia forces (i.e., the forces that develop at the floor and roof levels as a result of the acceleration of the floor and roof masses) corresponding to five of the largest peaks on the base-shear time-history shown in Fig. 12(a) (numbered P1 through P5). P1 corresponds to the dynamic maximum base shear, $V_{max,d}$. For comparison, the lateral forces corresponding to $V_{max,s}$ are shown by the dashed line in Fig. 12(b). The location of the resultant of each set of forces is shown by a solid circular marker.

The distribution of the lateral forces corresponding to $V_{max,s}$ is essentially a first mode distribution. The resultant of these forces is located at $0.78h_w$ from the base of the wall, where h_w is the height of the wall. The resultant of the inertia forces corresponding to $V_{max,d}$ (i.e., P1) is located at $0.27h_w$ from the base of the wall (significantly lower than $0.78h_w$). The static maximum base shear, $V_{max,s}$, can be related to the dynamic maximum base shear, $V_{max,d}$, using the base moment capacity of the wall, M_b: $V_{max,s} = M_b / 0.78h_w$ and $V_{max,d} = M_b / 0.27h_w$. Thus, $V_{max,d}$ is roughly 2.9 times $V_{max,s}$. This difference is attributed to the effect of higher modes (with shorter periods and lower resultant heights) which contribute significantly to the inertia forces.

For a wall responding in the nonlinear range, the increase in the base shear demand, V_{max}, due to the higher modes cannot be estimated accurately from a linear-elastic modal analysis procedure such as the one described in NEHRP.[9] This is because the effect of higher modes on the maximum base shear increases significantly due to the nonlinear behavior of the wall. Nonlinear behavior results in a decrease in the lateral stiffness (softening) which results in an elongation of the modal periods. Period elongation often results in an increase in the contribution of the higher modes to the inertia forces. Thus, the contribution of the higher modes to the base shear increases and can be comparable to the contribution of the first mode.

The proposed design approach includes a method to estimate the maximum base shear demand under the survival level ground motion, accounting for the effect of higher modes in the nonlinear range of response.[6] This method is based on a method developed by Kabeyasawa[12] and Aoyama[13] for cast-in-place reinforced concrete walls. The thick dashed horizontal lines in Fig. 12(a) indicate the expected maximum base shear demand, V_{max}, estimated using this method. Fig. 12(c) shows a comparison between V_{max} and the dynamic maximum base shear $V_{max,d}$ obtained from the analyses of Wall WH1 under 15 ground motion records scaled to 1.0g. The horizontal axis of Fig. 12(c) is the maximum incremental velocity of the ground motions. The maximum incremental velocity of a ground motion is equal to the maximum area under the acceleration time-history of the ground motion between two zero crossings. The results indicate that V_{max} provides a good upper bound to $V_{max,d}$.

Shear slip capacity, V_{ss} — The expected minimum shear slip capacity, V_{ss} of an unbonded post-tensioned precast wall is calculated as the product of the coefficient of shear friction, μ along the base-panel-to-foundation joint and the compression force acting through the joint.[6] In the design of the prototype walls, the coefficient of shear friction, μ, was assumed to be 0.7 as specified by the ACI 318 Code[10] for joints between precast members. The compression force acting through the base-panel-to-foundation joint was taken as the sum of the axial force due to gravity and the total post-tensioning steel force.

A minimum total post-tensioning steel force was used to calculate V_{ss} considering a reduction in the initial total post-tensioning steel force (i.e., prestress) due to the inelastic straining of the steel. The minimum total post-tensioning steel force was calculated assuming that the wall displaces, in both directions, to Δ_{sur}. This is described in more detail by Kurama et al.[6]

Fig 12(d) shows the shear-slip capacity time-history (solid lines) of Wall WH1 under the Newhall ground motion scaled to 1.0g. The shear slip capacity time-history is calculated using $\phi_s\mu = 0.6$. The shear slip capacity varies during the ground motion because the total post-tensioning steel force varies as shown in Fig. 11(a). The minimum shear slip capacity is reached when the minimum total post-tensioning steel force is reached. The dashed line in Fig. 12(d) shows the base-shear time-history of the wall [the same with Fig. 12(a)]. The most critical time for shear slip occurs at around 6 seconds when the maximum base shear, $V_{max,d}$, is reached just before the minimum shear slip capacity is reached. At this time, the shear slip capacity exceeds the base shear indicating that shear slip does not occur.

It is noted that additional work on the estimation of the shear slip capacity is needed. The coefficient of shear friction of the base-panel-to-foundation joint in an unbonded post-tensioned precast wall may be smaller than 0.7 as a result of the high compression stresses that occur in the joint due to post-tensioning and gap opening. Furthermore, the shear slip capacity of the joint may degrade under cyclic loading. Therefore, it is recommended that a conservative value of the coefficient of shear friction be used in design.

CURRENT RESEARCH

Currently, a large-scale experimental evaluation of the lateral load behavior of unbonded post-tensioned precast walls is being conducted at Lehigh University. Nine half-scale six-story wall specimens are being tested under combined gravity loading and cyclic lateral loading. Based on the results of these tests, the lateral load behavior of the walls will be evaluated and the shear slip capacity of the walls will be quantified.

The current research at the Leheigh University is funded by the National Science Foundation under Grant No. CMS-9612165, with substantial support from the precast concrete industry which has donated the test specimens and test fixtures, and has provided technical support for the design of the test specimens.

More recently, an analytical investigation of the effect of large openings (in the wall panels) on the seismic behavior and design of unbonded post-tensioned precast walls has been initiated at the University of Notre Dame. The openings can accommodate doors, windows, and mechanical penetrations which may be needed due to architectural or functional requirements.

The current research at the University of Notre Dame is funded in part by the Precast/Prestressed Concrete Institute by a 1998-1999 Daniel P. Jenny Research Fellowship. Detailed finite element models of the walls are being developed using the ABAQUS program. These models will be verified based on experimental results obtained at Lehigh University and will be used to investigate the effect of large openings in the walls.

CONCLUSIONS

The research summarized in this paper shows that unbonded post-tensioned precast walls provide a feasible alternative to conventional monolithic cast-in-place concrete walls in seismic regions. Conclusions regarding the seismic behavior and design of the walls are presented below.

1. Unbonded post-tensioned precast walls have the ability to soften and undergo large nonlinear lateral drift with little damage. As a result, only minor repair to the walls may be needed after a design level ground motion.

2. The nonlinear drift occurs primarily due to the opening of gaps along the horizontal joints.

3. Because little damage occurs in the walls, the behavior of the walls under cyclic lateral load is nearly nonlinear-elastic.

4. Unbonded post-tensioned precast walls can be designed to resist design level ground motions with little damage, and to resist severe survival level ground motions with damage, but without collapse. Design guidelines and requirements to obtain this behavior are presented in the paper.

5. Accurate estimates of the maximum lateral drift demands under design level and survival level ground motions are needed for design. The method used to estimate the maximum drift demands in the proposed design approach needs to be improved.

6. Nonlinear dynamic time-history analyses show that, as a result of the

nearly nonlinear-elastic behavior, an unbonded post-tensioned precast concrete wall has larger lateral drift under earthquake loading than a comparable cast-in-place reinforced concrete wall. However, an unbonded post-tensioned precast wall has significantly smaller residual drift (at the end of the ground motion) than a cast-in-place wall.

7. Shear slip along the horizontal joints is not a desired mode of lateral displacement. Shear slip under severe survival level ground motions can be prevented using the proposed design approach.

8. Inelastic straining of the post-tensioning steel during a ground motion results in a reduction in the total post-tensioning steel force. This reduction significantly affects the hysteretic behavior of the walls and results in a reduction in the shear slip capacity. The design approach includes a method to estimate the reduction in the total post-tensioning steel force under survival level ground motions.

RECOMMENDATIONS

Preliminary design recommendations are described in the paper. These include recommendations regarding the selection of the wall design properties (e.g., initial stress in the post-tensioning steel, total area of the post-tensioning steel, wall length, unbonded length of the post-tensioning steel, location of the post-tensioning steel, amount of spiral reinforcement) to achieve the design capacities as required by the proposed design approach. Design examples and more comprehensive design recommendations are expected to be developed based on the current experimental and analytical research.

The dynamic analysis results indicate that the equal displacement assumption can be used to estimate the maximum roof drift demands for walls designed for sites with a stiff soil profile but not for sites with medium or soft soil profiles. Improved methods to estimate the maximum roof drift demands for sites with medium and soft soil profiles are expected to be developed and incorporated into the proposed design approach based on current research.

Shear slip along the horizontal joints is prevented by requiring that the minimum shear slip capacity of the base-panel-to-foundation joint is larger than the maximum base shear demand. The paper proposes a method to estimate the maximum base shear demand including the effect of higher modes, and a method to estimate the minimum shear slip capacity including the reduction in prestress due to inelastic straining of the post-tensioning steel. It is recommended that a conservative value of the coefficient of shear friction be used in design. Further recommendations regarding the shear slip capacity are expected to be developed based on the current experimental research.

ACKNOWLEDGMENTS

The investigation was funded by the National Science Foundation (NSF) under Grant No. BCS-9307880 as part of the PREcast Seismic Structural Systems (PRESSS) research program. The support of the NSF Program Director Dr. S. C. Liu and Program Coordinator Dr. M. J. N. Priestley is gratefully acknowledged.

The authors also wish to thank several individuals for their assistance in the conduct of this work: K. Baur, High Concrete Structures, Inc.; M. Bertolini, Blakeslee Prestress, Inc.; N. Cleland, Blue Ridge Design, Inc.; T. D'Arcy, The Consulting Engineers Group, Inc.; H. Gleich, Metromont Materials Corporation; P. Johal, Precast/Prestressed Concrete Institute; S. Nakaki, Englekirk and Nakaki, Inc; H. Wilden, H. Wilden & Associates, Inc.; K. Jacob and N. Barstow, Lamont-Doherty Geological Observatory.

The authors appreciate the thoughtful comments provided by the reviewers. The opinions, findings, and conclusions expressed in the paper are those of the authors and do not necessarily reflect the views of the NSF or the individuals and organizations acknowledged above.

REFERENCES

1. Mueller, P., "Experimental Investigation on the Seismic Performance of Precast Walls," Ninth World Conference on Earthquake Engineering, Tokyo-Kyoto, Japan, V. IV, 1988, pp. 755-760.
2. Oliva, M., Clough, R., and Malhas, F., "Seismic Behavior of Large Panel Precast Concrete Walls: Analysis and Experiment," PCI JOURNAL, V. 34, No. 5, September-October 1989, pp. 42-66.
3. Hutchinson, R., Rizkalla, S., Lau, M., and Heuvel, S., "Horizontal Post-Tensioned Connections for Precast Concrete Load-bearing Shear Wall Panels," PCI JOURNAL, V. 36, No. 6, November-December 1991, pp. 64-76.
4. Priestley, M.J.N., "Overview of PRESSS Research Program," PCI JOURNAL, V. 36, No. 4, July-August 1991, pp. 50-57.
5. Kurama, Y., Pessiki, S., Sause, R., Lu, L.W., and El-Sheikh, M., "Analytical Modeling and Lateral Load Behavior of Unbonded Post-Tensioned Precast Concrete Walls," Research Report No. EQ-96-02, Department of Civil and Environmental Engineering, Lehigh University, Bethlehem, PA, November 1996, 191 pp.
6. Kurama, Y., Sause, R., Pessiki, S., Lu, L.W., and El-Sheikh, M., "Seismic Design and Response Evaluation of Unbonded Post-Tensioned Precast Concrete Walls," Research Report No. EQ-97-01, Department of Civil and Environmental Engineering, Lehigh University, Bethlehem, PA, November 1997, 184 pp.
7. Allen, M., and Kurama, Y., "Lateral Load Behavior and Design of Unbonded Post-Tensioned Precast Walls with Large Openings," in preparation for submittal to the PCI JOURNAL, 1999.
8. El-Sheikh, M., Sause, R., Pessiki, S., and Lu, L.W., "Seismic Behavior and Design of Unbonded Post-Tensioned Precast Frames," PCI JOURNAL, V. 44, No. 3, May-June 1999.
9. Building Seismic Safety Council, "NEHRP Recommended Provisions for the Development of Seismic Regulations for New Buildings," BSSC, Washington, D.C., 1991, 1994, 1997.
10. ACI Committee 318, "Building Code Requirements for Structural Concrete (ACI 318-95) and Commentary (ACI 318R-95)," American Concrete Institute, Farmington Hills, MI, 1995, 369 pp.